Orientation of Pigeonite Exsolution Lamellae in Metamorphic Augite: Correlation with Composition and Calculated Optimal Phase Boundaries

Howard W. Jaffe, Peter Robinson, Robert J. Tracy,

*Department of Geology, University of Massachusetts,
Amherst, Massachusetts 01002*

AND Malcolm Ross

U.S. Geological Survey, Reston, Virginia 22092

Abstract

Optical examination of metamorphic augites coexisting with orthopyroxenes ranging in composition from Fs_{15} to Fs_{95} from the Adirondacks, the Hudson Highlands, and the Cortlandt Complex, New York, and the Belchertown Complex, Massachusetts, shows three sets of exsolution lamellae. X-ray single crystal photographs show these are orthopyroxene lamellae on (100), and pigeonite lamellae, termed "001" and "100", oriented on irrational planes near (001) and (100). Optically observed angles of the phase boundaries of "001" and "100" lamellae with respect to the c axis of host augite vary with iron-magnesium ratio determined from electron probe analyses of 29 pyroxenes, supplemented by 76 measurements of gamma index of refraction. The angles are largest in magnesian specimens and are in near agreement with angles of optimal phase boundaries calculated from measured lattice parameters of host and one or both sets of pigeonite lamellae. Compositional control of lamellae orientation is related to compositional control of lattice parameters, which appear not to have changed significantly since exsolution in the range 800-500°C.

Introduction

Many igneous and metamorphic rocks contain pyroxenes which have unmixed during cooling. The exsolved pyroxenes form as lamellae which have been generally described in the past as being oriented parallel to the (100) or (001) lattice planes of the host (Poldervaart and Hess, 1951). Metamorphic augites containing sets of exsolution lamellae in three different orientations were first described by Jaffe and Jaffe (1973)[1] from their occurrence in augite-orthopyroxene granulites and amphibolites associated with Precambrian crystalline gneisses of the Monroe quadrangle in the Hudson Highlands of New York (Fig. 1). These authors noted that only one of the three sets of lamellae was parallel to a crystallographic axis, the c axis, of the host augite, whereas the two more prominent sets of pigeonite were not parallel to the (001)

and (100) directions of the host, as had been generally accepted (Poldervaart and Hess, 1951). These significant relations were established solely by petrographic microscopic study of grain mounts by noting that the obtuse angle between the two prominent sets of lamellae was 122° rather than the 105–106° required by two sets of lamellae parallel to (001) and (100) of augite.

Subsequently, a study of these exsolution phenomena in more detail by Robinson, Jaffe, Ross, and Klein (1971)[1] established by single crystal X-ray photographs that the lamellae parallel to (100) of the augite host were orthopyroxene. They found that the two more prominent sets of lamellae, designated as "001" and "100" lamellae, were indeed pigeonite[2] with phase boundaries, separating lamel-

---

[1] The paper by Jaffe and Jaffe (1973) was submitted for publication in 1969, but not published until 1973 because of a freeze on funds at the N.Y. State Museum and Science Service. It thus preceded the study and publication of the paper by Robinson, Jaffe, Ross, and Klein (1971).

[2] The definitions of pigeonite and augite used here are based partly on the work of Ross, Huebner, and Dowty (1973). Pigeonite is defined as a monoclinic pyroxene containing less than 20 mole percent $CaSiO_3$ component (Wo < 20). The $FeSiO_3$ component can vary from zero to 100 mole percent, although for the end-members only, we would use the names clinoenstatite (En_{100}) and clinoferrosilite (Fs_{100}). Pigeonite can be unambiguously identified by single
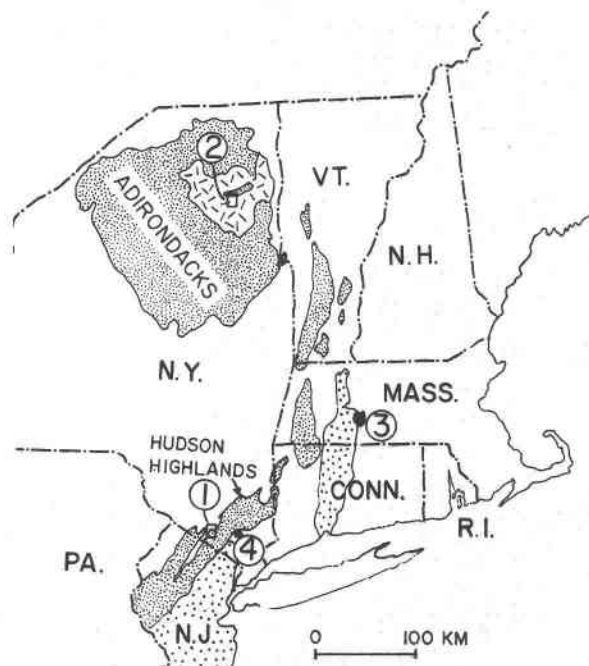
EXPLANATION

	Mesozoic and Cenozoic Cover
	Belchertown, Cortlandt Complexes
	Paleozoic
	Anorthosite
	Precambrian

FIG. 1. Generalized geologic map showing locations from which coexisting pyroxenes were obtained: (1) Monroe quadrangle, Hudson Highlands; (2) Mount Marcy quadrangle, Adirondacks; (3) Belchertown Complex; (4) Eastern part of the Cortlandt Complex.

lae from host, that are not oriented parallel to a specific rational lattice plane of the host. These authors also demonstrated that the orientation of exsolution lamellae of pigeonite in augite, and also that of monoclinic amphiboles in each other, was in accordance with the optimal phase boundary theory

crystal X-ray diffraction by (1) its space group symmetry $P2_1/c$ at room temperature, and (2) by having a β angle of greater than $107.5°$ (usually $108-109°$) at room temperature. The names clinoenstatite, clinobronzite, clinohypersthene, and clinoferrosilite are not used for naturally occurring pyroxenes because there is no consensus on the range of Fs or Wo content to be attached to those names. Some would prefer to call a clinopyroxene of composition Wo_{10} (En, Fs)$_{90}$ "pigeonite" but would call a clinopyroxene

of Bollmann, as applied to exsolution in feldspars by Bollmann and Nissen (1968).

Soon thereafter, a study of grain immersion mounts revealed that the exsolution phenomena discovered in the two-pyroxene granulites of the Hudson Highlands, described above, are even more widespread in two-pyroxene-bearing anorthosites, granulites, and charnockitic gneisses in the Mount Marcy quadrangle of the Adirondacks. Detailed measurements of the gamma indices of refraction of orthopyroxenes coexisting with these clinopyroxenes indicated a wide range of iron-magnesium ratios—namely, 100 $(Fe^{2+} + Fe^{3+} + Mn)/(Mg + Fe^{2+} + Fe^{3+} + Mn)$—from 40 to 95 (Table 1, Fig. 2). Pyroxene assemblages richer in magnesium were obtained from the Belchertown Intrusive Complex of central Massachusetts (Fig. 1; Emerson, 1898, 1917; Guthrie and Robinson, 1967; Guthrie, 1972; Hall, 1973) and the Cortlandt ultramafic complex of southeastern New York (Fig. 1; Shand, 1942; Tracy, 1970). Measurements of the gamma index of refraction of orthopyroxenes from these rocks indicated iron-magnesium ratios of 15 to 35 (Table 1). Thus pyroxene pairs were available for study in which the orthopyroxenes range in composition from Fs_{15} to Fs_{95} (Fig. 2). In all cases these orthopyroxenes coexisting with augite contain augite exsolution lamellae parallel to (100).

Although of different primary origins, all of the pyroxene pairs under discussion are believed to have equilibrated under generally similar metamorphic conditions of high temperature, intermediate pressure, and low humidity equivalent to the granulite facies. Hudson Highlands and Adirondack specimens appear to have been involved in Precambrian granulite facies metamorphism of regional extent, although the Adirondack specimens also contain some relict features of earlier plutonic events. The specimens from the Belchertown Complex came from a Devonian batholith. Subsequent to syntectonic emplacement, the batholith underwent hydration during continued regional metamor-

of composition Wo_2 (En, Fs)$_{98}$ clinohypersthene. Yet pigeonite on cooling may unmix enough augite to give it this low calcium content.

Augite is defined as a clinopyroxene having greater than 20 mole percent $CaSiO_3$ (Wo > 20) and Fs content from zero to 80 mole percent. Augite is unambiguously identified by having space group symmetry $C2/c$ and a β angle of less than $107.5°$ (usually $105.5-106.5°$). The names diopside and hedenbergite are reserved for the augite end-members $CaMgSi_2O_6$ and $CaFeSi_2O_6$ respectively.
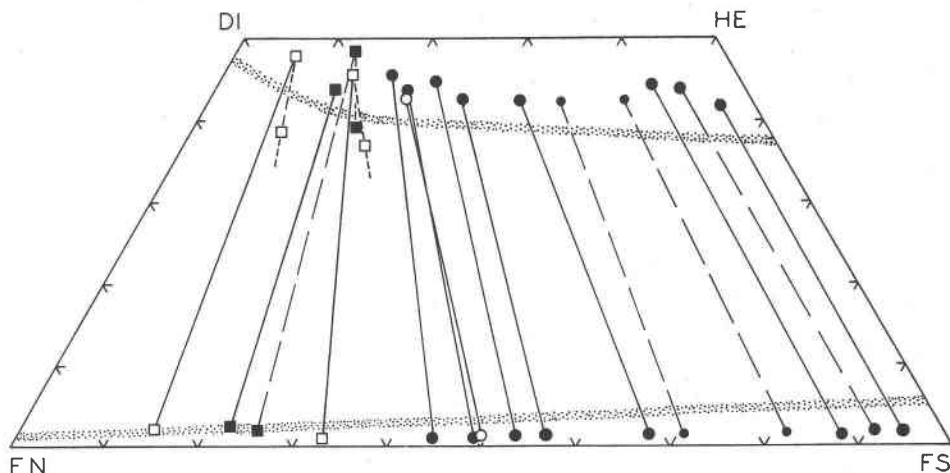
FIG. 2. Compositions of co-existing pyroxenes from the Hudson Highlands (open circles), Adirondacks (closed circles), Belchertown Complex (open squares), and Cortlandt Complex (closed squares). All compositions were determined by electron probe, except for those marked by the smaller closed circles, which were determined optically. Solid tie lines indicate specimens for which X-ray single crystal data have been obtained; long-dashed tie lines, only optical data on exsolution lamellae. Short-dashed lines indicate trend of zoning in augites 447, T65, and A21. Stippled pattern indicates limits of mutual solid solution of synthetic Ca-Mg-Fe augite and orthopyroxene at 810°C as determined by Lindsley, King, and Turnock (1974).

phism that left the central core with the relict granulite facies mineralogy of an orthopyroxene-augite monzodiorite. The interior of the eastern end of the Ordovician Cortlandt Intrusive Complex seems also to have preserved essentially granulite facies assemblages although undergoing recrystallization during later regional metamorphism (Tracy, 1970). Further detail concerning the specimens and their geologic setting is given in the Appendix.

Optical Properties and Composition of Pyroxenes

The compositions of coexisting pyroxenes in 38 specimens were estimated by measurement of indices of refraction in immersion oils (Table 1) and verified by thirteen sets of electron probe analyses (Table 2). Optical curves based on the new probe analyses (Figs. 3, 4) proved more reliable than curves based on literature data and were used for all optically determined compositions reported in this paper.

Orthopyroxene

Measurement of the gamma index of refraction of orthopyroxenes in fragment mounts is simple because both the excellent {210} cleavage and the good {100} parting provide numerous plates oriented with the Z-vibration direction parallel to the

stage of the microscope. According to Deer, Howie, and Zussman (1963), each atomic percent of $(Fe^{2+} + Fe^{3+} + Mn)$ leads to an increase of 0.00125 in the gamma index of refraction of orthopyroxenes from both igneous and metamorphic parageneses. This correlation incorporates data for orthopyroxenes from plutonic rocks (Hess, 1952, 1960), from volcanic rocks (Kuno, 1954), and from high-grade metamorphic rocks (Muir and Tilley, 1958; Howie, 1955), all of which are plotted on Figure 3. Electron probe and optical data obtained during this study show less scatter and a new curve relating iron-magnesium ratios with gamma indices of refraction was constructed (Fig. 3). This was used to obtain the iron-magnesium ratios listed in parentheses in Table 1.

Augite

Ordinarily, one measures the beta index of refraction of augite in order to obtain an estimate of the iron-magnesium ratio as suggested by Hess (1949). However, an evaluation of the optical data for analyzed augites listed by Hess (1960) and Deer *et al* (1963) shows that the gamma index of refraction yields estimates of the iron-magnesium ratios comparable to those obtained from the beta index. It is much more informative and convenient

TABLE 1. Optical Measurements of Angles of Exsolution Lamellae of Pigeonite in Host Augite, γ Indices of Refraction, and Compositions of Coexisting Pyroxenes from the Adirondacks, Hudson Highlands, Belchertown Complex, and Cortlandt Complex*

Sample	γ-Aug	fe^{**}-Aug		γ-Opx	fe^{**}-Opx		"001"∧c	"100"∧c	"100"∧"001"

ADIRONDACKS, N. Y.[#]

Sample	γ-Aug	fe^{**}-Aug		γ-Opx	fe^{**}-Opx		"001"∧c	"100"∧c	"100"∧"001"
Nk	1.715		(26)	N.D.			116.5°	10°	126.5°
Ph-3	1.717		(29)	1.714		(40)	N.D.	12°	
Al	1.717		(29)	1.718		(43)	119°	11.5°	130.5°
Ma-5	1.7175		(30)	1.720		(44)	117°	7.5°	124.5°
MD-1	1.7195		(32)	1.718		(43)	117°	11°	128°
Jo-8	1.720	33.0	(33)	1.720	44.8	(44)	117°	12°	129°
Pr-1	1.720		(33)	1.720		(44)	117°	12°	129°
Go-4	1.720	36.5	(33)	1.727	49.2	(49)	115°	8°	123°
Sb-2	1.724		(39)	1.727		(49)	116°	9°	125°
Po-1	1.726	41.8	(42)	1.733	53.9	(54)	117°	7°	124°
S1-5	1.726		(42)	1.7295		(51)	115.5°	8.5°	124°
Ma-3	1.727		(44)	1.729		(51)	115°	7°	122°
VH-2	1.727		(44)	1.730		(51)	116.5°	8.5°	125°
Ca-6	1.729	46.9	(47)	1.738	57.1	(57)	115°	5°	120°
CD	1.733		(53)	1.738		(57)	115°	6°	121°
Ca-17	1.736	57.5	(57)	·1.752	68.1	(68)	112.5°	3°	115.5°
Giant#	1.736		(57)	1.759		(74)	113°	2°	115°
JB-2	1.741		(65)	1.757		(72)	112°	1°	113°
Go-2	1.746		(72)	1.773		(85)	111.5°	0.5°	112°
Sb-1	1.7485		(76)	1.771		(83)	111.5°	0.5°	112°
Po-13	1.7505	82.7	(79)	1.7760	88.9	(88)	111.5°##	0°	111.5°
SC-6	1.759	87.5	(92)	1.785	92.3	(96)	111°##	0°	111°
Po-17	1.760	93.4	(93)	1.786	95.5	(97)	111°##	0°	111°

HUDSON HIGHLANDS, N. Y.

Sample	γ-Aug	fe^{**}-Aug		γ-Opx	fe^{**}-Opx		"001"∧c	"100"∧c	"100"∧"001"
J515	1.713		(23)	1.717		(42)	115°	9°	124°
J241S	1.716		(27)	1.715		(40)	115°	10°	125°
J223	1.720	36.4	(33)	1.729	50.1	(51)	116°	6°	122°
J437P	1.722		(36)	1.731		(52)	114°	6°	120°

BELCHERTOWN, MASS.

Sample	γ-Aug	fe^{**}-Aug		γ-Opx	fe^{**}-Opx		"001"∧c	"100"∧c	"100"∧"001"
447	1.704	12.9	(9)	1.682	14.5	(16)	122°	22°	144°
115	1.714		(24)	1.703		(32)	119°	13°	132°
110	1.714		(24)	1.704		(32)	119.5°	12.5°	132°
113	1.716		(27)	1.7025		(31)	120°	13°	133°
A21	1.716	26.1	(27)	1.705	33.3	(33)	120°	12.5°	132.5°

CORTLANDT COMPLEX, N. Y.

Sample	γ-Aug	fe^{**}-Aug		γ-Opx	fe^{**}-Opx		"001"∧c	"100"∧c	"100"∧"001"
T62	1.7075		(14)	1.693		(24)	120°	16°	136°
T58	1.708		(15)	1.6935		(25)	122°	17°	139°
T25	1.714		(24)	1.703		(32)	119°	16°	135°
T52	1.718	23.1	(30)	1.696	22.8	(26)	122.5°	19.5°	142°
T65	1.724	24.0	(39)	1.702	25.7	(31)	123°	17°	140°

* All microscopic measurements by H. W. Jaffe.

** $fe = 100(Fe^{2+}+Fe^{3+}+Mn)/(Mg+Fe^{2+}+Fe^{3+}+Mn)$ determined by electron probe analysis (underlined) or optically using Figure 3 or Figure 4, this paper.

[#] Adirondack specimens except Giant are from Mount Marcy 15' quadrangle. Giant is from adjoining Elizabethtown quadrangle.

Recent optical re-examination of Po-13, SC-6 and Po-17 has revealed a very very fine second set of "001" pigeonite lamellae oriented at 112°, 112.5°, and 112.5° respectively. These appear to represent a second episode of exsolution at lower temperature, similar to second and third sets of "001" lamellae observed in some igneous augites (Ross, Robinson, and Jaffe, 1972).

FIG. 3. Variation of the γ index of refraction and the ratio 100 $(Fe^{2+} + Fe^{3+} + Mn)/(Mg + Fe^{2+} + Fe^{3+} + Mn)$ for orthopyroxenes. Data from Deer, Howie, and Zussman (1963) and present study (labelled points). Indices of pure synthetic enstatite (1.658) and orthoferrosilite (1.789) from Stephenson, Sclar, and Smith (1966) and Lindsley, MacGregor, and Davis (1964), respectively. Solid curve fitted visually to data points of present study (except T65) and synthetic end members. Dashed line is linear least squares best fit of same data points. The equation for this line is:

$$n\gamma = 1.6626 + 0.1297 \, [(Fe^{2+} + Fe^{3+} + Mn)/$$
$$(Mg + Fe^{2+} + Fe^{3+} + Mn)].$$

to measure the gamma index because grains that lie parallel to the optic plane (010) yield, in addition to the gamma index of refraction: (1) maximum relief between exsolution lamellae and host, (2) maximum exsolution angles, "001" ∧ c and "100" ∧ c, and (3) the relative orientation of the Z-vibration direction with respect to exsolution lamellae and the c-crystallographic axis (see Jaffe, Robinson, and Klein, 1968). Neither β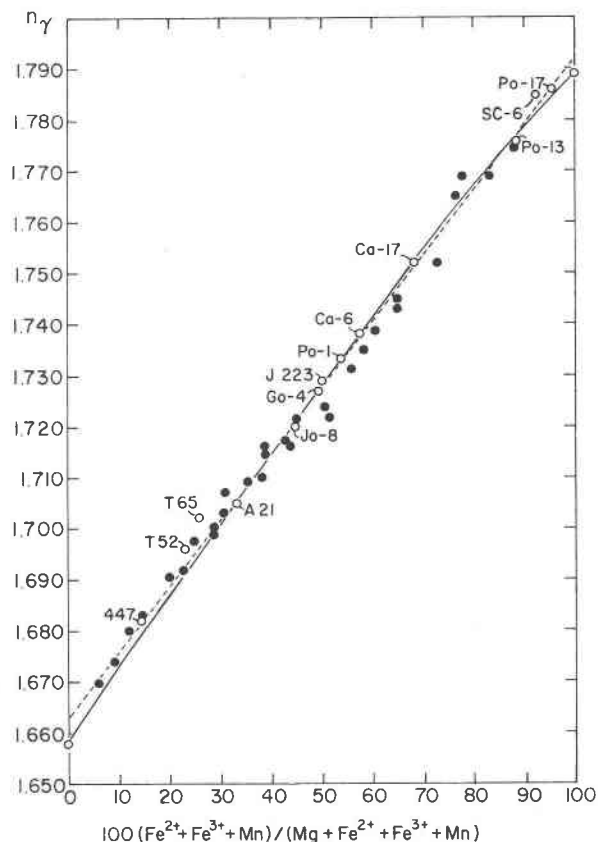 or γ, however, yields accurate iron-magnesium ratios due to the extensive substitution of Al^{IV}, Al^{VI}, Fe^{3+VI}, Ti^{VI}, and Na^{VIII} in augites, and a plot of published data (Fig. 4) shows a considerable scatter of points. Electron probe and optical data obtained during this study show much less scatter and a new curve relating iron-magnesium ratios with gamma indices of refraction was constructed (Fig. 4). This was used to obtain the iron-magnesium ratios listed in parentheses in Table 1.
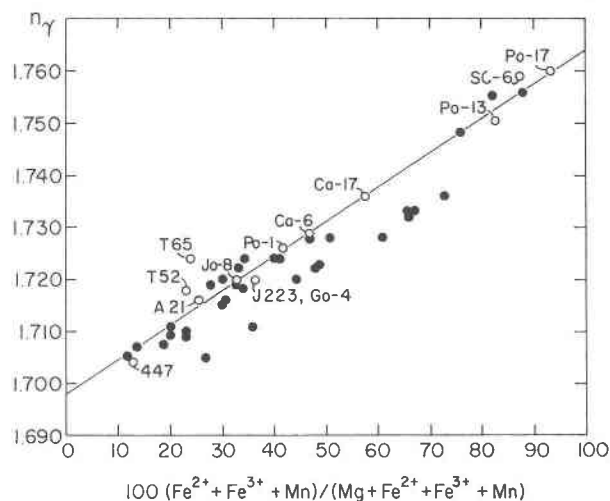
FIG. 4. Variation of the γ index of refraction with the ratio $100\ (Fe^{2+} + Fe^{3+} + Mn)/(Mg + Fe^{2+} + Fe^{3+} + Mn)$ in augites coexisting with orthopyroxene. Data from Hess (1960); Deer, Howie, and Zussman (1963); and present study (labelled points). Line is both visual and least squares best fit to data points of present study, excluding T65. Equation for line is:

$$n\gamma = 1.6977 + 0.0669\ [(Fe^{2+} + Fe^{3+} + Mn)/(Mg + Fe^{2+} + Fe^{3+} + Mn)].$$

Composition of Coexisting Pyroxenes

Electron probe analyses and structural formulae of coexisting pyroxenes are listed in Table 2 and presented graphically in Figure 2. In doing the analyses an effort was made to avoid putting the electron beam on large concentrations of exsolution lamellae. When the beam was deliberately aimed at concentrations of lamellae, the analysis usually gave some intermediate composition along the tie line connecting augite and orthopyroxene compositions. Thus, in general, analyses with maximum and minimum ca^3 values were considered to represent the compositions of the augite and orthopyroxene, respectively, on which the optical measurements were made. Exceptions to this occurred in augites 447, T65, and A21 (Fig. 2) in which analyses on apparently clear grains yielded a range of ca^3 values between distinct upper and lower limits. The analyses, with low ca^3 values of 38.7, 39.1, and 37.0 respectively, can be interpreted in two ways: (a) they represent distinct primary chemical zoning in these metamorphosed igneous augites, or (b) they represent analyses of places on the polished surface of the augite crystal occupied by thin

---

[3] $ca = 100Ca/(Ca + Mg + Fe + Mn)$

pigeonite lamellae parallel to the surface. In all three examples (Fig. 2), the chemical zoning trend of augite lies on the Fe-rich side of the augite-orthopyroxene tie line. This suggests that pigeonite lamellae are more Fe-rich than the coexisting orthopyroxene, but does not rule out the possibility of primary zoning, which is supported in the case of 447 by some variation in the index of refraction (1.700 to 1.704). In this case the highest index corresponding to the highest Ca content was employed for optical determinative work.

Keeping in mind the uncertainties discussed above, the ca^3 values from probe analysis of coexisting augite and orthopyroxene can be used to estimate temperature conditions of exsolution on the basis of experimental work in the pyroxene quadrilateral, particularly the 810°C isotherm (Fig. 2) of Lindsley, King, and Turnock (1974). Unfortunately, unlike the lunar specimens evaluated by these authors, only four of the specimens reported here contain less than 3 wt percent of "nonquadrilateral" components. Nevertheless, the plotted trends of the Adirondack specimens in Figure 2 are generally parallel to the experimental solvi and suggest temperatures of equilibration lower than 810°C.

As is to be expected, the orthopyroxene generally has a higher Fe/Mg ratio than the coexisting augite. Distribution of Fe and Mg between the coexisting pyroxenes may be described in terms of a distribution coefficient K_D (Kretz, 1963) where

$$K_D \begin{matrix}Opx-Aug \\ Mg-Fe\end{matrix} = \frac{(Mg/Fe + Mg)^{Opx}}{(Fe/Fe + Mg)^{Opx}} \cdot \frac{(Fe/Fe + Mg)^{Aug}}{(Mg/Fe + Mg)^{Aug}}$$

This simple formulation was employed in calculating the values of K_D in Table 3. More elaborate formulation involving consideration of full site occupancy (Saxena, 1971) was rejected at this time because of uncertainties in site assignment related to analytical uncertainties and inadequate knowledge of the oxidation state of Fe.

The effect of Fe^{3+} on K_D is illustrated by specimen A21, which is probably the most oxidized rock in the suite, in that the pyroxenes coexist with titanohematite. Wet chemical analyses of purified augite and orthopyroxene separates (Ashwal, 1974) yield ratios of $Fe^{3+}/Fe^{2+} + Fe^{3+}$ of 0.333 and 0.085 respectively, and a much lower K_D value (Table 3). Estimates of Fe^{3+} content can be made from electron probe analyses, by summing the formula to four cations, but this method is heavily dependent on

TABLE 2a. Electron Probe Analyses of Coexisting Pyroxenes

AUGITE

	447-1	447-2	T52	T65-1	T65-2	A21-1	A21-2	Jo-8	Go-4	J223	Po-1	Ca-6	Ca-17	Po-13	SC-6	Po-17
SiO_2	51.78#	52.40#	47.66*	47.17*	48.61*	51.47#	52.17#	49.88*	49.66*	50.29#	48.95*	49.04*	48.72*	47.17*	48.18*	47.53*
TiO_2	.33	.36	.36	1.61	1.66	.31	.10	.18	.18	.02	.21	.17	.16	.14	.08	.21
Al_2O_3	3.61	4.11	6.97	6.28	5.12	2.27	1.99	2.77	2.44	1.39	2.77	2.50	1.86	1.24	.89	1.08
Cr_2O_3	.98	.63	.29	.09	.15	.07	.02	.46	.62	.02	.44	.33	.18	.07	.00	.11
MgO	15.27	17.51	14.98	13.13	14.81	13.63	15.05	12.76	12.63	12.96	11.12	10.42	8.31	3.11	2.21	1.23
NiO			.23					.14	.08		.18	.18	.18	ZnO .24	.29	.46
FeO	3.84	5.68	7.70	7.21	10.12	8.35	11.47	10.92	12.52	12.49	14.01	16.12	19.51	26.04	27.47	30.39
MnO	.18	.09	.32	.19	.25	.23	.24	.29	.39	.75	.25	.29	.58	.31	.35	.44
CaO	22.52	18.22	21.10	22.45	18.43	21.20	17.72	22.15	21.56	21.11	21.62	20.24	19.91	19.68	19.24	18.29
BaO			.03					.03	.03		.02	.04	.03			
Na_2O	.93	.90	.67	.68	.65	.89	.85	.55	.68	.14	.77	1.05	.85	.78	.73	.57
K_2O			.03	.00	.00			.02	.03		.02	.02	.04	.00	.00	.00
Total	99.44	99.90	100.34	98.80	99.79	98.42	99.61	100.15	100.82	99.17	100.36	100.40	100.33	98.77	99.44	100.31

ORTHOPYROXENE

	447-1	447-2	T52	T65-1	T65-2	A21-1	A21-2	Jo-8	Go-4	J223	Po-1	Ca-6	Ca-17	Po-13	SC-6	Po-17
SiO_2	53.72*		51.37*	50.98*		52.55#		49.92*	48.97*	50.73#	48.17*	50.27*	48.05#	44.92*	46.05*	45.17*
TiO_2	.08		.14	.36		.03		.10	.11	.01	.12	.09	.06	.10	.12	.13
Al_2O_3	2.21		4.72	4.25		1.20		1.59	1.05	1.06	1.60	1.18	.69	.38	.26	.47
Cr_2O_3	.10		.05	.07		.03		.00	.16	.00	.15	.04	.00	.05	.07	.09
MgO	31.28		28.09	26.45		24.00		19.83	18.06	17.20	15.97	14.50	10.43	3.44	2.34	1.35
NiO	.15		.15					.04	.28		.05			ZnO .45	.56	.62
FeO	9.16		14.40	16.19		20.63		28.08	30.36	28.81	32.69	33.96	38.65	48.32	49.40	50.14
MnO	.32		.35	.21		.74		.58	.87	1.88	.50	.41	1.03	.82	.83	1.30
CaO	1.06		1.21	1.11		.46		.53	.60	.67	.74	.66	.68	.68	.72	.75
BaO	.00		.00					.02	.00		.04					
Na_2O	.10		.00	.12		.00		.04	.06	.01	.06	.00	.01	.00	.00	.08
K_2O	.03		.00	.00				.02	.02		.04	.00		.00	.00	.04
Total	98.21		100.48	99.75		99.64		100.75	100.54	100.37	100.13	101.11	99.60	99.16	100.35	100.14

*R.J. Tracy, analyst; on MAC Model 400 electron probe, using standard Bence-Albee correction procedures, at Institute of Materials Science, University of Connecticut, Storrs, except T65, Opx Ca-6, Po-13, SC-6, Po-17 at Department of Earth and Planetary Sciences, Massachusetts Institute of Technology.

#Nelson Hickling, analyst; on ARL-EMX electron probe, using standard correction procedures, at U.S. Geological Survey, Washington, D.C.

@Last three values in this row are for ZnO.

TABLE 3. Distribution Coefficients of Fe and Mg in Coexisting Augite and Orthopyroxene

Sample		Fe/Fe+Mg	K_D	Sample		Fe/Fe+Mg	K_D
447-1	Aug	.123	.854	Jo-8	Aug	.324	.603
	Opx	.141			Opx	.443	
447-2	Aug	.154	1.109	Go-4	Aug	.357	.590
	Opx	.141			Opx	.485	
447-1	Aug	.123	.771	J223	Aug	.351	.577
447-2	Aug	.154			Opx	.484	
T52	Aug	.224	1.000	Po-1	Aug	.414	.614
	Opx	.224			Opx	.535	
T65-1	Aug	.236	.897	Ca-6	Aug	.465	.661
	Opx	.256			Opx	.568	
T65-2	Aug	.277	1.113	Ca-17	Aug	.568	.633
	Opx	.256			Opx	.675	
T65-1	Aug	.236	.806	Po-13	Aug	.825	.601
T65-2	Aug	.277			Opx	.887	
A21-1	Aug	.256	.715	SC-6	Aug	.874	.586
	Opx	.325			Opx	.922	
A21-2	Aug	.299	.886	Po-17	Aug	.933	.671
	Opx	.325			Opx	.954	
A21-1	Aug	.256	.807				
A21-2	Aug	.299					
A21	Aug	.194	.559				
WET	Opx	.301					

the accuracy of the SiO_2 analysis and was not used for this paper.

It thus appears likely that much of the scatter of K_D values in the range 0.577 to 0.671 (specimens Jo-8 through Po-17) is a function of analytical difficulties. They are, however, all lower than the generalized value of $K_D = 0.690$ suggested for the 810°C isotherm by Lindsley et al (1974), and hence consistent with equilibration at a lower temperature. On the other hand, the extremely high values of K_D exhibited by specimens 447-1, T52, and T65-1 appear to be related to very high Al_2O_3 and/or TiO_2 content in augite, possibly combined with higher temperature of formation of these ultramafic rocks. The still higher values for 447-2 and T65-2 are related to the low ca^3 values of these augite analyses. If the interpretation is correct that these low Ca analyses are due to pigeonite exsolution lamellae, then they may be combined with the high Ca analyses to yield a K_D which might be interpreted as that between augite and pigeonite during the exsolution (Table 3).

The analyses of Table 2 permit generalizations

TABLE 2b. Formulas Per Six Oxygens for Coexisting Pyroxenes

	447-1	447-2	T52	T65-1	T65-2	A21-1	A21-2	Jo-8	Go-4	J223	Po-1	Ca-6	Ca-17	Po-13	SC-6	Po-17
AUGITE																
Si	1.909	1.909	1.776	1.784	1.822	1.948	1.955	1.891	1.884	1.931	1.880	1.895	1.914	1.946	1.978	1.962
Al	.091	.091	.224	.216	.178	.052	.045	.109	.109	.063	.120	.105	.086	.054	.022	.038
	2.000	2.000	2.000	2.000	2.000	2.000	2.000	2.000	1.993	1.994	2.000	2.000	2.000	2.000	2.000	2.000
Al	.066	.086	.082	.064	.048	.049	.043	.015			.005	.009		.006	.021	.014
Ti^{4+}	.009	.010	.010	.045	.046	.009	.003	.005	.005	.001	.006	.005	.005	.004	.002	.007
Cr^{3+}	.029	.018	.009	.002	.004	.002	.000	.014	.019	.001	.013	.010	.006	.002		.004
Mg	.839	.951	.832	.740	.827	.769	.841	.721	.714	.742	.637	.600	.487	.191	.136	.075
Ni		.007						.004	.002		.006	.006	.006	Zn .007	.009	.014
Fe^{2+}	.118	.173	.240	.228	.317	.264	.359	.346	.397	.401	.450	.521	.641	.899	.944	1.049
Mn^{2+}	.006	.003	.010	.005	.007	.007	.008	.009	.013	.024	.008	.009	.019	.011	.012	.015
Ca	.890	.711	.842	.909	.739	.859	.711	.900	.877	.869	.890	.838	.838	.870	.847	.809
Ba			.001						.001	.001		.000	.001	.001		
Na	.066	.064	.048	.049	.046	.065	.062	.040	.050	.010	.057	.079	.065	.062	.058	.046
K			.001					.001	.001			.000	.001	.002		
	2.023	2.016	2.082	2.042	2.034	2.024	2.027	2.056	2.079	2.048	2.072	2.079	2.071	2.052	2.029	2.033
fe**	12.9	15.6	23.1	24.0	28.1	26.1	30.4	33.0	36.5	36.4	41.8	46.9	57.5	82.7	87.5	93.4
ca##	48.0	38.7	43.8	48.3	39.1	45.3	37.0	45.5	43.8	42.7	44.8	42.6	42.2	44.1	43.7	41.5
ORTHOPYROXENE																
Si	1.924	1.846		1.857		1.953	1.908	1.906	1.959	1.901	1.959	1.962	1.954	1.982	1.967	
Al	.076	.154		.143		.047	.072	.048	.041	.074	.041	.033	.019	.013	.024	
	2.000	2.000		2.000		2.000	1.980	1.954	2.000	1.975	2.000	1.995	1.973	1.995	1.991	
Al	.018	.046		.039		.006			.007		.013					
Ti^{4+}	.002	.004		.009		.001	.003	.003	.000	.004	.002	.002	.003	.004	.004	
Cr^{3+}	.003	.001		.001		.001		.005		.005	.000		.002	.003	.003	
Mg	1.670	1.504		1.436		1.329	1.129	1.048	.990	.939	.842	.635	.223	.150	.088	
Ni	.004	.004					.001	.009		.002			Zn .014	.018	.020	
Fe^{2+}	.274	.433		.493		.641	.898	.988	.930	1.079	1.107	1.320	1.758	1.778	1.826	
Mn^{2+}	.010	.011		.005		.023	.019	.029	.062	.017	.012	.036	.030	.030	.048	
Ca	.041	.047		.042		.018	.022	.025	.028	.031	.027	.030	.032	.033	.035	
Ba									.000		.001					
Na	.007			.008			.003	.005	.001	.005		.001			.006	
K	.001						.001	.001		.002					.002	
	2.030	2.050		2.033		2.019	2.076	2.113	2.018	2.085	2.003	2.024	2.062	2.016	2.032	
fe**	14.5	22.8		25.7		33.3	44.8	49.2	50.1	53.9	57.1	68.1	88.9	92.3	95.5	
ca##	2.0	2.3		2.1		1.0	1.0	1.2	1.4	1.5	1.3	1.5	1.6	1.7	1.8	

** fe = 100(Fe+Mn)/(Fe+Mn+Mg)
ca = 100 Ca/(Ca+Fe+Mn+Mg)
@ Last three values in this row are for Zn.

concerning the behavior of several other elements. Mn is concentrated in orthopyroxene over augite, as is Zn in the three specimens analyzed. Cr, Al, and Ti, with rare exceptions, are strongly preferred in augite over orthopyroxene. Na, without exception, follows Ca in augite.
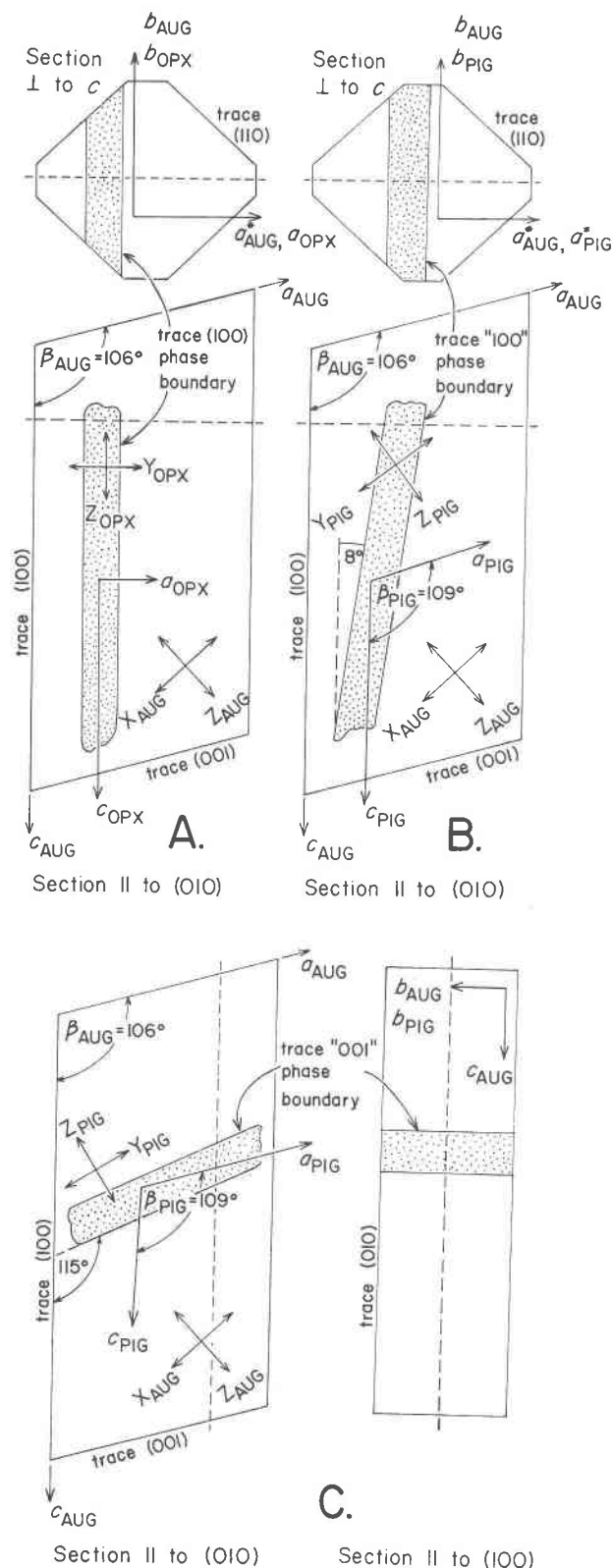
Exsolution Lamellae in Augite

Crystallographic Orientation

The relative lattice orientations of host augite and the three types of unmixed pyroxenes, (100) orthopyroxene, "100" pigeonite, and "001" pigeonite, were determined by single crystal precession photography to an accuracy of ±0.1 to 0.2 degrees. Orthopyroxene and "100" pigeonite (Fig. 5A and 5B, respectively) are oriented so that their *b* and *c*

axes are parallel or nearly parallel to *b* and *c*, respectively, of the host augite. These two pyroxenes thus are oriented with their (010) and (100) planes parallel to those of augite. The "001" pigeonite (Fig. 5C) is oriented with its *a* and *b* axes parallel or nearly parallel to *a* and *b* axes respectively, of the augite; the (001) and (010) planes of both phases being parallel. A slight divergence of the *a* or *c* axes of host augite and exsolved pigeonite (0.25 to 0.45°), due to lattice rotation about the common *b* direction, was observed in four specimens (Table 4), and is discussed below.

X-ray single crystal precession photographs were taken of eleven representative specimens from a wide range of compositions from which lattice parameters, relative orientations, and relative amounts of lamellar phases were determined (Table 4). The low con-

tent of pyroxene lamellae in most of the specimens necessitated long exposure times, in some cases up to 200 hours before reflections of lamellar phases could be satisfactorily observed. In spite of this, in the more magnesian specimens (447, T52, A21, Jo-8, Go-4, Po-1), in all of which both "001" and "100" pigeonite lamellae were detected optically, only the "100" pigeonite lamellae were sufficiently abundant to yield a measurable diffraction pattern. Similarly, three of the specimens (A21, J223, Ca-6) showed no trace of orthopyroxene (100) lamellae although such lamellae could be seen optically.

In nearly all cases the lamellar pyroxenes appear to have an identical b dimension to the host augite, or at least so close to the host that it cannot be separately resolved. The single exception is specimen Po-13 in which the b dimension of orthopyroxene lamellae is slightly smaller than b of the host. In those single crystals in which lattice parameters for both "001" and "100" pigeonite lamellae were obtained (J223, Ca-6, Ca-17, Po-13, Po-17), the two sets of lamellae may have slightly different a, c, and β values. It is not known whether these differences are due to differences in chemical composition, or represent physical constraint on the parameters of the lamellae by the host. In pyroxenes from high temperature lunar basalts, Ross, Huebner, and Dowty (1973) noted that the "001" lamellae within host augites and host pigeonites have their a dimensions constrained to a of the host, whereas the "100" lamellae have their c dimensions constrained to c of the host.

Morphological Orientation

All of the unmixed pyroxenes in augite grew as lamellae 0.2 to 3.0 μm thick, the contacts of

Fig. 5. Crystallographic, morphological, and optical orientations of exsolution lamellae (stippled) in augite. **A.** Augite with (100) orthopyroxene lamella. $a_{AUG} \wedge a_{OPX} = 16°$, $b_{AUG} \wedge b_{OPX} = 0°$, $c_{AUG} \wedge c_{OPX} = 0°$. Phase boundary of orthopyroxene lamella is parallel to (100) of augite. **B.** Augite with "100" pigeonite lamella. $a_{AUG} \wedge a_{PIG} \simeq 3°$, $b_{AUG} \wedge b_{PIG} = 0°$, $c_{AUG} \wedge c_{PIG} \simeq 0°$. Phase boundary of pigeonite lamella is parallel to b, but at an 8° angle to c of augite ("100" $\wedge c_{AUG} = 8°$). **C.** Augite with "001" pigeonite lamella. $a_{AUG} \wedge a_{PIG} \simeq 0°$, $b_{AUG} \wedge b_{PIG} = 0°$, $c_{AUG} \wedge c_{PIG} \simeq 3°$. Phase boundary of pigeonite lamella is parallel to b, but at a 115° angle to c of augite ("001" $\wedge c_{AUG} = 115°$).

which are referred to as *phase boundaries*. The morphological orientations of the phase boundaries of the three types of exsolved lamellae were determined by optical examination of single augite crystal fragments in immersion oils. Orientations are most successfully measured in grains oriented with (010) parallel to the stage and immersed in an oil of refractive index close to that of the host. In this position the lamellae are viewed edge on, indicating, within the accuracy of optical measurements, that they are parallel to the *b* axis of the augite host. Because the phase boundaries are oriented parallel or nearly parallel to *b* of the augite, their absolute orientation may be defined by the angle between the trace of the lamellae as seen in the (010) plane and the *c* direction of the augite. These angles are designated "100" ∧ *c* for "100" pigeonite, and "001" ∧ *c* for "001" pigeonite.

Orthopyroxenes (Fig. 5A) are oriented so that the phase boundary is always parallel to the (100) plane of the augite. The "100" pigeonite lamellae possess phase boundaries that deviate from being parallel to (100) of the host by 0 to 22° (Table 4). An example of "100" pigeonite with "100" ∧ *c* = 8° is shown in Figure 5B. The "001" pigeonite lamellae have phase boundaries which deviate from the (001) plane of augite by 5 to 17° ("001" ∧ *c* = 111° to 123°, Table 4). An example of "001" pigeonite with "001" ∧ *c* = 115° is shown in Figure 5C. Where "001" pigeonite is in an orientation so that the phase boundary is parallel to (001) of augite, "001" ∧ *c* = β augite.

Measurement of the angles of exsolution lamellae was accomplished to a precision of ±1° on crystal fragments oriented with (010) perpendicular to the optical axis of the microscope. Such grains are also most suitable for measuring the gamma index of refraction and the angle between the *Z* vibration direction and the *c* axis. The *c* direction of augite could usually be found by observing either the trace of the {110} cleavage or the trace of the (100) orthopyroxene exsolution lamellae.

The orientation of the phase boundaries of the "001" pigeonite exsolution lamellae is defined by the *obtuse* angle ("001" ∧ *c*) measured between the *c* axis of the host and the trace of the lamellae on (010). The orientation of the phase boundaries of the "100" pigeonite exsolution lamellae is defined by the *acute* angle ("100" ∧ *c*) measured between the *c* axis of the host and the trace of the

lamellae on (010). In examples considered in this paper, the angle between the trace of the "100" lamellae and the *a* axis of the host, and the angle between the trace of the "001" lamellae and the *c* axis of the host is greater than the β angle of augite. Both sets of lamellae thus lie "in the acute angle β" (Robinson *et al*, 1971, Fig. 5-1, 5-4). In some amphiboles and pyroxenes these angles are less than the β angle of the host so that the lamellae lie "in the obtuse angle β" (Robinson *et al*, 1971, Fig. 5-3, 5-6; Ross, Robinson, and Jaffe, 1972). In grains lacking both "100" orthopyroxene lamellae and {110} cleavage traces, the angle between the "100" and "001" lamellae ("100" ∧ "001") may be measured as a separate but related angle.

Relation to Composition

The exsolution features under consideration were first studied in augites of intermediate Fe/Mg ratio from the Hudson Highlands (Table 1) with "001" angles of 114–116° and "100" angles of 6–10° (Fig. 6B). Pyroxenes of similar composition from the Adirondacks showed similar or slightly larger angles (Table 1). With increasing iron content in the Adirondack specimens the angles of both "001" and "100" lamellae decrease (Fig. 6C, 6D) until for the most iron-rich specimen obtained, an augite for which *fe* = 93.5, the "001" angles are 111° and the "100" pigeonite lamellae are parallel to the *c* axis. Since the most magnesian Adirondack pyroxene pair has augite *fe* = 33, more magnesian pyroxene pairs, believed to have formed under similar conditions, were sought and found in the Belchertown and Cortlandt Complexes (Table 1). The most magnesian and most dramatic of these is specimen 447 (Fig. 6A) with angles of 122° and 22° and a total angle between the two sets of pigeonite lamellae of 144°.

The relations between the composition of augite and angles of pigeonite exsolution lamellae in all augite specimens from Table 1 are summarized in Figure 7. The two insets in each part illustrate schematically typical patterns involving the two pertinent sets of lamellae for magnesian and iron-rich compositions. Figure 7 shows moderate scatter and some interesting differences between the Hudson Highlands and Adirondack specimens, and among the Cortlandt specimens; these may represent either differences in composition or differences in conditions of formation. Overall the correlation between
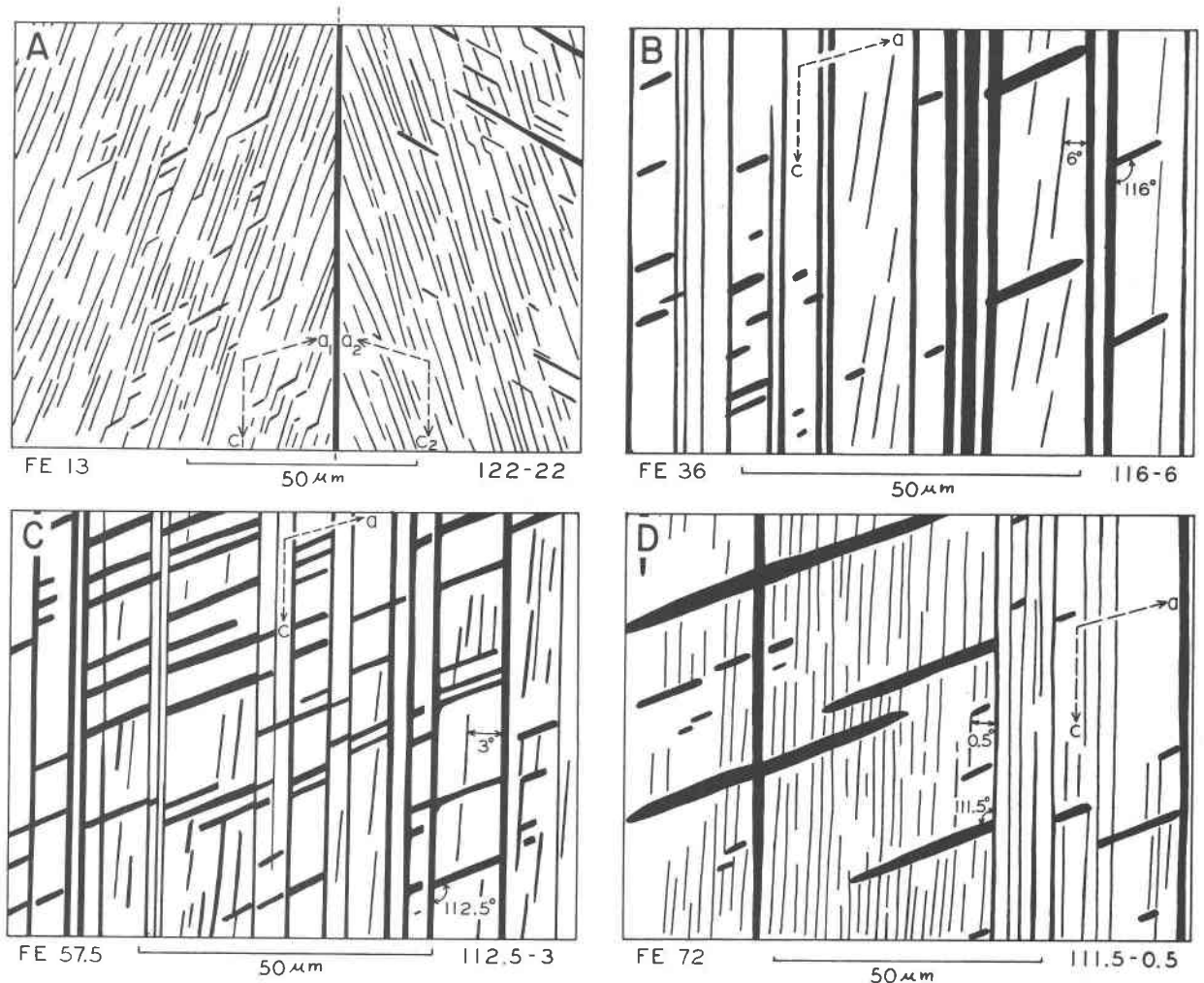
FIG. 6. Tracings from photomicrographs of augites with different iron-magnesium ratios showing patterns and angles of exsolution lamellae. Scale and directions of augite a and c crystallographic axes indicated. FE indicates value of the ratio 100 $(Fe^{2+} + Fe^{3+} + Mn)/(Mg + Fe^{2+} + Fe^{3+} + Mn)$ from Table 1.

A. Specimen 447 from Belchertown Complex. Crystal twinned on (100) with single orthopyroxene lamella on twin plane. Thin and thick stubby lamellae are pigeonite "001" lamellae at 122° to the c axis. Thin abundant lamellae forming herringbone pattern across twin plane are pigeonite "100" lamellae at 22° to the c axis. (b axis is nearly normal to plane of paper, but slightly misoriented, so that angles shown are slightly less than maximum observed angles of 122° and 22°.)

B. Specimen J223 from Hudson Highlands (original photomicrograph is Fig. 1 of Robinson et al, 1971). Coarse vertical lamellae are (100) orthopyroxene. Thick stubby lamellae are "001" pigeonite at 116° to the c axis. Very thin lamellae are "100" pigeonite at 6° to the c axis.

C. Specimen Ca-17 from Adirondacks. Vertical lamellae are (100) orthopyroxene. Thick stubby lamellae are "001" pigeonite at 112.5° to the c axis. Thin lamellae are "100" pigeonite at 3° to the c axis.

D. Specimen Go-2 from Adirondacks. Thick vertical lamellae are (100) orthopyroxene. Thick tapered lamellae are "001" pigeonite at 111.5° to the c axis. Very thin lamellae are "100" pigeonite at 0.5° to the c axis.

composition and angle of exsolution lamellae is excellent. Indeed, in routine thin section petrography reasonably careful measurements of exsolution lamellae in metamorphic augites can be applied to Figure 7 to yield rough estimates of Fe/Mg ratio.

Figure 8 is similar to Figure 7 but shows the angles of pigeonite exsolution lamellae in augite plotted against the composition of the coexisting orthopyroxene. This has some practical value because the composition of orthopyroxene can be more accurately estimated from optical data. It can be justified only to the extent that the composition of the coexisting orthopyroxene resembles the composition of the pigeonite lamellae that participated
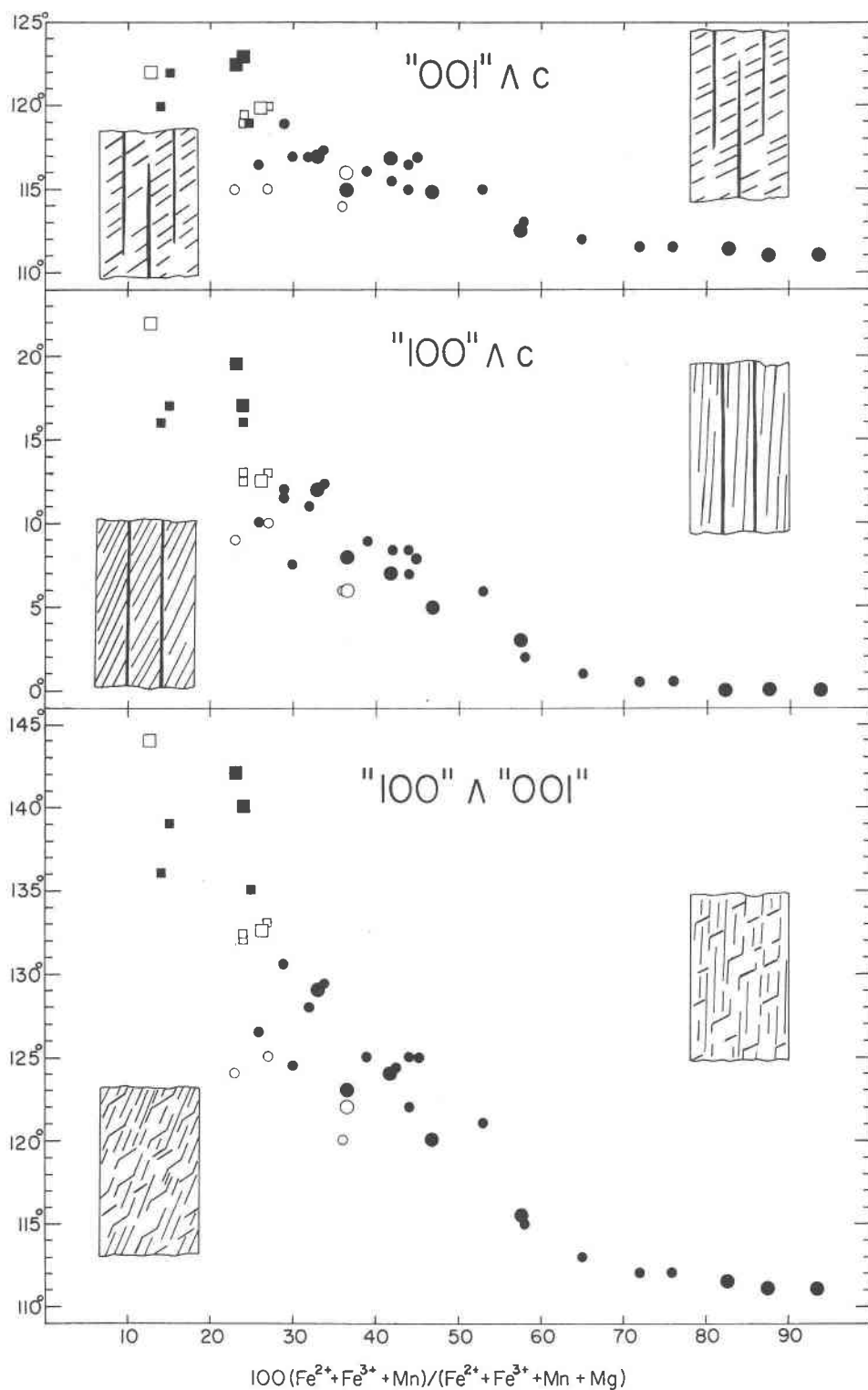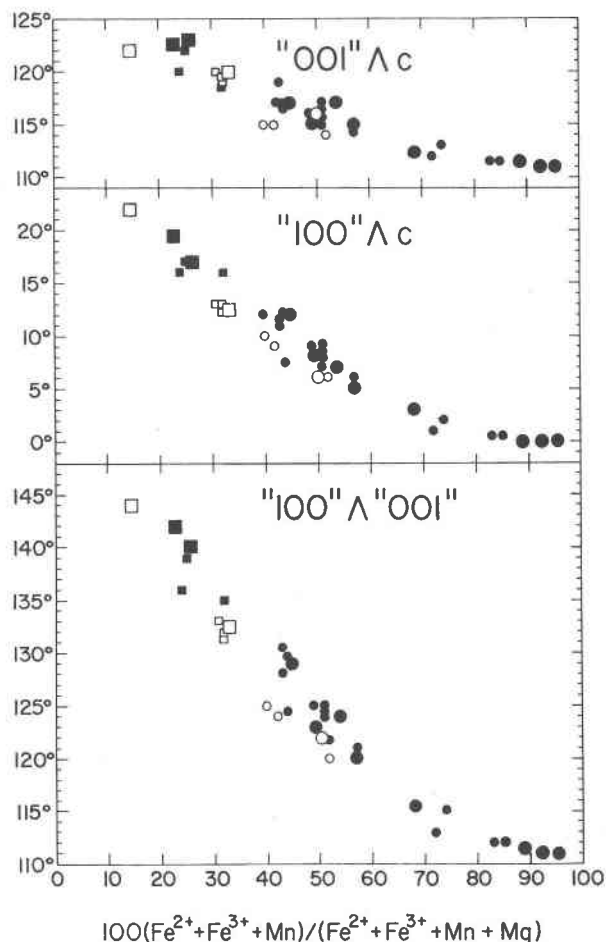
FIG. 7. Angles of pigeonite exsolution lamellae in metamorphic augites plotted against 100 $(Fe^{2+} + Fe^{3+} + Mn)/(Fe^{2+} + Fe^{3+} + Mn + Mg)$ of augite determined by electron probe analyses (large symbols) or by measurement of the gamma index of refraction (small symbols). Insets to left and right show some exsolution patterns of Mg-rich and Mg-poor augites respectively. Closed circles: Mt. Marcy area, Adirondacks. Open circles: Monroe quadrangle, Hudson Highlands. Closed squares: Cortlandt Complex, New York. Open squares: Belchertown Intrusive Complex, Central Massachusetts.

FIG. 8. Angles of pigeonite exsolution lamellae in metamorphic augites plotted against 100 $(Fe^{2+} + Fe^{3+} + Mn)/(Fe^{2+} + Fe^{3+} + Mn + Mg)$ of coexisting orthopyroxene. Plot is justified to the extent that orthopyroxene mimics the composition of pigeonite that was involved in the exsolution process. Symbols same as in Figure 7.

equally with augite in the exsolution process. The pigeonite and orthopyroxene lamellae observed in the present study are much too thin to analyze quantitatively with the electron probe. In the one case from the Bushveld Complex where probe analyses could be made of both hosts and lamellae (Boyd and Brown, 1969), host orthopyroxene and pigeonite lamellae in augite have fairly similar compositions.

Calculated Optimal Phase Boundaries

According to the principle of "optimal phase boundaries" (Bollmann, 1970; Bollmann and Nissen, 1968), when two lattices are superimposed in space

there will be planes of dimensional best fit between the lattices that in nature tend to form the boundary between them. In the case of simple monoclinic lattices with identical b dimensions and fairly similar a and c dimensions, and β angles, very slight relative rotations about the b axis will produce optimal phase boundaries that are perfect with respect to the dimensional position on the boundary surface of equivalent points in the two lattices (Robinson et al, 1971). The orientation of these optimal phase boundaries can be calculated with reasonable accuracy from any pair of lattice parameters using simple trigonometric equations programmed for computer (check Robinson, Jaffe, Ross, and Klein, Erratum, 1971).

The qualitative effects of relative variations in the a and c dimensions on the orientation of "001" and "100" lamellae have been covered previously (Robinson et al, 1971). Based on computer calculations, the quantitative effects of variation in a and c dimensions and of the β angle are shown in Figure 9. It should be emphasized that the absolute values of the parameters are much less important than their differences or misfit (symbolized Δ). If c and β are held constant at 5.27 Å and 109° for augite and 5.22 Å and 105° for pigeonite, the angle "001" $\wedge$ c for "001" lamellae increases markedly with Δa (Fig. 9, left) whereas the angle "100" $\wedge$ c for "100" lamellae hardly changes at all. If a and β are held constant at 9.76 Å and 109° for augite and at 9.68 Å and 105° for pigeonite, however, "100" $\wedge$ c changes markedly with Δc but "001" $\wedge$ c does not (Fig. 9, center). For a and c held constant, the angles of both sets of exsolution lamellae—that is, "100" $\wedge$ c and "001" $\wedge$ c—increase markedly as $\Delta\beta$ decreases (Fig. 9, right). This last effect was not emphasized in our previous work, but its geometric sense may be deducible from study of Figure 4 of Robinson et al (1971).

Figure 10 shows, for analyzed augites, the Δa's, Δc's, and $\Delta\beta$'s from the lattice parameters (Table 4) plotted against the iron-magnesium ratios. Despite some scatter, the general picture is clear. The magnesian pyroxenes have larger angles of exsolution lamellae because they have *larger* a and c misfits and also because they have *smaller* $\Delta\beta$'s (see Smith, 1969, p. 23). Even without the lattice parameters presented in Table 4, this was deduced by calculating "best fit" exsolution angles for the synthetically matched pure end member pairs diopside-clinoenstatite $(CaMgSi_2O_6-Mg_2Si_2O_6)$ (127°,
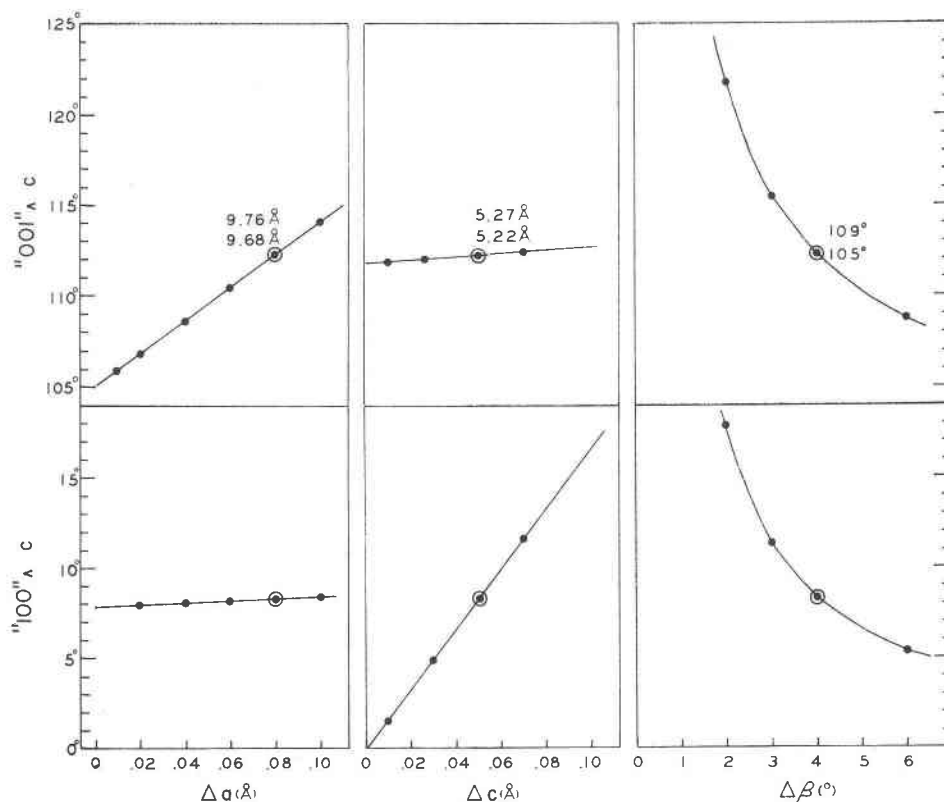
Fig. 9. Quantitative effect of variation of differences in *a, c,* and *β* (Δ*a,* Δ*c,* Δ*β*) on the angles of "001" and "100" pigeonite exsolution lamellae. Pairs of values at double circle denote representative absolute values of the indicated parameter (*a* at left, *c* at center, *β* at right) for augite (upper value) and pigeonite (lower value). These values also were the ones held constant when varying a parameter in each of the other columns. Left column: effect of variation of "*a* misfit" (Δ*a*), with *c* and *β* of augite and pigeonite held constant at 5.27 and 5.22, and at 105° and 109°, respectively. Center column: effect of variation of "*c* misfit" (Δ*c*), with *a* and *β* of augite and pigeonite held constant at 9.76 and 9.68, and at 105° and 109°. Right column: effect of variation of Δ*β*, with *a* and *c* of augite and pigeonite held constant at 9.76, 9.68, and 5.27, 5.22, respectively.

22°) and hedenbergite-clinoferrosilite (CaFeSi$_2$O$_6$-Fe$_2$Si$_2$O$_6$) (117°, 4°) (Robinson *et al,* 1971, Table 3, Nos. 1 and 3). It is dramatically shown in plots of *a* and *c* dimensions for synthetic pyroxenes in the Di-Hed-Clinoen-Clinofs quadrilateral (Turnock, Lindsley, and Grover, 1973).

The results of calculations of optimal phase boundaries are given in Table 4. For each pair of lattice parameters, for example, augite host and pigeonite "100" lamellae, orientations are calculated both for "100" lamellae and also for hypothetical "001" lamellae (in parentheses) with identical lattice parameters. For augites for which lattice parameters have been measured for both pigeonite "001" and "100" lamellae, two pairs of orientations

are calculated: from pigeonite "100" parameters, "100" actual and "001" hypothetical; from pigeonite "001" parameters, "001" actual and "100" hypothetical. It will be noted that for the many specimens in which only pigeonite "100" lamellae were sufficiently abundant to obtain lattice parameters, the calculated hypothetical "001" orientations are close to the optically measured orientations of "001" lamellae.

Figure 11 gives a comparison of calculated and observed angles of exsolution lamellae in the pyroxenes in Table 4. Despite some scatter the correlation is excellent and gives very strong confirmation that the lamellae did indeed form on optimal phase boundaries. Slight differences between observed and

TABLE 4.   Metamorphic Augites and Included Exsolution Lamellae: Lattice Parameters from X-Ray Single Crystal Photographs, Calculated Optimal Phase Boundaries, and Calculated and Observed Lattice Rotations

Sample	Aug fe*		a	b	c	β	w	Diff. from β	Angle	Meas. Angle	Rotation** Calc.	Rotation** Obs.	w	Angle	Meas. Angle	Rotation## Calc.	Rotation## Obs.
									"001" LAMELLAE						"100" LAMELLAE		
447	12.9	Augite host (90%)	9.726	8.874	5.253	106.11°											
		Pigeonite "100" (10%)	9.621	"	5.193	108.61°	(1.60)#	(16.5°)	(122.6°)	122°	(.42°)		5.18	17.4°	22°	.43°	.42±.05°
		Orthopyroxene(100)(tr)															
T52	23.1	Augite host (80%)	9.738	8.882	5.275	106.03°											
		Pigeonite "100" (20%)	9.644	"	5.205	108.62°	(1.86)	(14.5°)	(120.6°)	122.5°	(.39°)		4.65	19.0°	19.5°	.45°	.45±.1°
		Orthopyroxene(100)(tr)															
A21	26.1	Augite host (90%)	9.748		5.262	105.95°											
		Pigeonite "100" (10%)	9.659		5.214	108.73°	(2.30)	(12.0°)	(117.9°)	120°	(.29°)		7.91	12.0°	12.5°	.29°	.28±.05°
Jo-8	33.0	Augite host (80%)	9.743	8.914	5.255	105.95°											
		Pigeonite "100" (5%)	9.649	"	5.217	108.62°	(2.12)	(12.9°)	(118.8°)	117°	(.28°)		9.67	9.9°	12°	.24°	.0±.1°
		Orthopyroxene(100)(15%)	18.28	"	5.222												
Go-4	36.5	Augite host (90%)	9.755	8.914	5.249	105.91°											
		Pigeonite "100" (4%)	9.666	"	5.227	108.58°	(2.34)	(11.7°)	(117.6°)	115°	(.22°)		17.50	5.7°	8°	.13°	.0±.1°
		Orthopyroxene(100)(6%)	18.30	"	5.245												
J223	36.4	Augite host (90%)	9.776	8.390	5.252	105.91°											
		Pigeonite "100" (5%)	9.694	"	5.248	108.83°	(2.94)	(9.5°)	(115.4°)		(.16°)		111.34	.9°	6°	.03°	.0±.2°
		Pigeonite "001" (2%)	9.695	"	5.236	108.55°	2.60	10.7°	116.6°	116°	.19°	.25±.1°	(24.36)	(4.1°)		(.10°)	
Po-1	41.8	Augite host (80%)	9.759	8.936	5.266	105.92°											
		Pigeonite "100" (10%)	9.682	"	5.239	108.63°	(2.76)	(10.1°)	(116.0°)	117°	(.20°)		14.54	6.8°	7°	.16°	.0±.1°
		Orthopyroxene(100)(10%)	18.33	"	5.256												
Ca-6	46.9	Augite host (90%)	9.749	8.914	5.264	106.02°											
		Pigeonite "100" (3%)	9.671	"	5.236	108.73°	(2.71)	(10.3°)	(116.3°)		(.21°)		13.94	7.0°	5°	.16°	.0±.2°
		Pigeonite "001" (7%)	9.699	"	5.232	108.73°	4.32	6.6°	112.7°	115°	.14°	.0±.2°	(12.50)	(7.8°)		(.15°)	
Ca-17	57.5	Augite host (77%)	9.770	8.943	5.256	105.48°											
		Pigeonite "100" (5%)	9.693	"	5.236	108.80°	(3.50)	(8.1°)	(113.6°)		(.18°)		24.98	4.0°	3°	.10°	.0±.2°
		Pigeonite "001" (8%)	9.716	"	5.227	108.78°	4.97	5.8°	111.3°	112.5°	.14°	.0±.2°	(17.21)	(5.8°)		(.14°)	
		Orthopyroxene(100)(10%)	18.40	"	5.249												
Po-13	82.7	Augite host (84%)	9.782	8.976	5.252	105.40°											
		Pigeonite "100" (4%)	9.706	"	5.256	108.50°	(3.45)	(8.2°)	(113.6°)		(.13°)		100	-0.9°	0°	-.02°	.0±.2°
		Pigeonite "001" (8%)	9.724	"	5.236	108.48°	4.38	6.5°	111.9°	111.5°†	.12°	.0±.2°	(29.52)	(3.4°)		(.07°	
		Orthopyroxene(100)(4%)	18.42	8.972	5.246												
Po-17	93.4	Augite host (85%)	9.787	9.002	5.245	105.42°											
		Pigeonite "100" (5%)	9.742	"	5.245	108.53°	(5.90)	(4.9°)	(110.3°)		(.08°)		∞	0.0°	0°	.00°	.0±.2°
		Pigeonite "001" (5%)	9.725	"	5.233	108.40°	3.97	7.2°	112.6°	111°†	.13°	.0±.2°	(38.2)	(2.7°)		(.05°)	
		Orthopyroxene(100)(5%)	18.43	"	5.242												

* Composition of augite host; fe = 100(Fe+Mn)/(Fe+Mn+Mg) determined by electron probe analysis (Table 2).

Parentheses indicate values calculated from "hypothetical lamellae" (see text).

** Relative counter-clockwise rotation of lattice of pigeonite "001" lamellae with respect to (001) of augite host.

Relative clockwise rotation of lattice of pigeonite "100" lamellae with respect to (100) of augite host.

† Recent optical re-examination of Po-13 and Po-17 has revealed a very very fine second set of "001" pigeonite lamellae oriented at 112° and 112.5° respectively. These appear to represent a second episode of exsolution at lower temperature, similar to second and third sets of "001" lamellae observed in some igneous pyroxenes (Ross, Robinson and Jaffe, 1972). The observed angles of these late fine lamellae of 112° and 112.5° agree most closely with angles of 111.9° and 112.6° calculated from lattice parameters.

calculated angles of "100" lamellae could be due to changes in parameters since exsolution, particularly reduction of Δc; but at the moment this interpretation is highly speculative. From the evidence at hand the relative lattice parameters appear to have changed only very slightly since exsolution took place.

Lattice Rotation

In our earlier paper (Robinson *et al*, 1971) and above, we pointed out that slight relative rotation of pyroxene lattices allowed improvement of the fit between lattices. We also presented in detail the qualitative effect of relative parameters on the direction of relative lattice rotation. In the examples we evaluated earlier, this rotation as calculated from lattice parameters was so small, generally 0.15° or less, that it could not be accurately measured in precession photographs.[4] It was natural, then, to seek evidence for such lattice rotation in the more magnesian specimens with large exsolution angles, and in this we were successful.

Detection and measurement of lattice rotation in X-ray single crystal photographs is dependent on size of crystal used and abundance of lamellae. Small angular separations of spots only show up in photographs of small undistorted crystals. In many

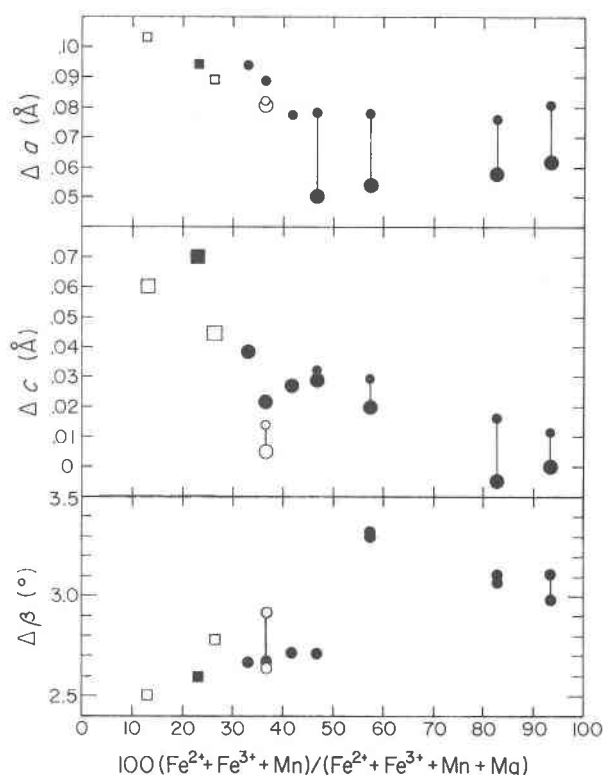[4] Precision in measuring angular relationships from the X-ray precession photographs is 0.05° to 0.2°.

FIG. 10. Δa's, Δc's, and $\Delta \beta$'s from X-ray single crystal data in Table 4 plotted against $100 \ (Fe^{2+} + Fe^{3+} + Mn)/(Fe^{2+} + Fe^{3+} + Mn + Mg)$ of augite host. Vertical lines connect data points derived from single crystals in which lattice parameters for two sets of pigeonite lamellae were obtained. In Δa row large symbols indicate "actual" values derived from parameters of "001" lamellae, small symbols indicate "hypothetical" values derived from parameters of "100" lamellae. In Δc row large symbols indicate "actual" values derived from parameters of "100" lamellae, small symbols indicate "hypothetical" values derived from parameters of "001" lamellae. Δa and Δc are larger, and $\Delta \beta$ is smaller with lower iron content, resulting in larger angles of exsolution lamellae.

FIG. 11. Comparison of optically observed angles of "001" and "100" pigeonite exsolution lamellae in augites with angles calculated from measured lattice parameters for several different iron-magnesium ratios. Vertical lines connect observed and calculated values for a single specimen. Solid circle: Optically observed angle of exsolution lamellae. Thick cross bar: Calculated angle based on lattice parameters of "actual" lamellae. Thin cross bar: Calculated angle based on lattice parameters of "hypothetical" lamellae. Double cross bars: Calculated angle for "001" $\wedge$ "100" based on combination of "actual" and "hypothetical" results.

such crystals exsolution lamellae are not sufficiently abundant to give measurable X-ray reflections, hence larger crystals must necessarily be used with resultant loss of definition. For these reasons, in the majority of cases, small lattice rotations could be neither detected nor ruled out, but the evidence for lattice rotation is decisive in four cases (Table 4).

It will be seen that for "001" lamellae, *calculated* rotations all fit into case 1-1 of Figure 6 (earlier paper) with relative counter-clockwise rotation of pigeonite lattices. Of the four augites in which X-ray reflections of "001" pigeonite lamellae were obtained, the most magnesian (J223) shows relative

counter-clockwise rotation of the "001" pigeonite lattice of $0.25 \pm 0.1°$ (case 1-1) in close agreement with the calculated value of $0.19°$. For "100" lamellae *calculated* rotations all fit into case 4-1 of Figure 6 (earlier paper) with relative clockwise rotation of pigeonite lattices, except for Po-13 which, by $0.02°$, is in case 6-1 with counter-clockwise rotation. The augites from the three most magnesian specimens (447, T52, and A21) show relative clockwise rotations (case 4-1) of $0.42 \pm 0.05°$, $0.45 \pm 0.1°$

and $0.28 \pm 0.05°$ in close agreement with calculated rotations of $0.43°$, $0.45°$, and $0.29°$ respectively. Thus in the four cases where lattice rotations are large enough to be detected, they are in remarkably good agreement with rotations calculated independently from lattice parameters. This agreement is a further confirmation of the optimal phase boundary theory.

Notation of Phase Boundaries

In this paper we have used the notations "001" and "100" to designate the relative orientation of the crystal lattices of the host and unmixed phase. As we have previously stated, the phase boundaries of these "001" and "100" lamellae are not usually parallel to the (001) or (100) host lattice plane. Thus, in the general case, the "001" or "100" phase boundary plane must be described as being parallel to an irrational lattice plane.

In Table 4, in addition to the calculated angles of "001" and "100" exsolution lamellae and the differences from β for "001" lamellae, a number w is listed for each calculated orientation. The value w is the non-integral number that represents the position in the first row of lattice points above the origin that is common to both lattices (Robinson *et al*, 1971, p. 923). Another way to look at this is that w is the irrational intercept of an "001" phase boundary on the a axis when the intercept is 1 on the c axis or vice versa for "100" boundaries. "Miller" indices for the phase boundaries may be derived from these irrational intercepts. Because "001" boundaries may have either positive or negative intercepts on a, and "100" boundaries, positive or negative intercepts on c depending on the relative values of a_{AUG} and a_{PIG}, and c_{AUG} and c_{PIG} respectively (Robinson *et al*, 1971, Fig. 5), the orientation of the lamellae with respect to both lattices may be accurately described in terms of the irrational Miller indices as shown in Table 5. The interested reader may wish to ink in the appropriate Miller indices in each of the six sections of Figure 5 in the earlier paper.

Comment on Equilibrium Relations During Crystallization and Exsolution of Metamorphic Augite

Implicit in the work on igneous augites of Poldervaart and Hess (1951, p. 483), Hess (1960, p. 40), Preston (1966, p. 1230), Boyd and Brown (1968, p. 358; 1969, p. 212), and Smith (1969, p. 24)

TABLE 5. Relation between Relative Lattice Parameters, Irrational Intercepts, and Irrational Miller Indices of Phase Boundaries in Monoclinic Pyroxenes

	$a_{AUG} > a_{PIG}$			$a_{AUG} = a_{PIG}$			$a_{AUG} < a_{PIG}$		
Intercepts	+w	∞	1	∞	∞	1	−w	∞	1
Miller Indices	1	0	w	0	0	1	$\bar{1}$	0	w

	$c_{AUG} > c_{PIG}$			$c_{AUG} = c_{PIG}$			$c_{AUG} < c_{PIG}$		
Intercepts	1	∞	+w	1	∞	∞	1	∞	−w
Miller Indices	w	0	1	1	0	0	$\bar{w}$	0	1

is the idea that pigeonite exsolves from augite only under temperature conditions where pigeonite is the stable Ca-poor pyroxene above the pigeonite-orthopyroxene inversion loop. In the case of the specimens considered here, the metamorphic Ca-poor pyroxene coexisting with augite is orthopyroxene. The paucity and fine scale of exsolution lamellae in these specimens show that the initial solid solution was very limited as compared to igneous pyroxene pairs of similar iron-magnesium ratio, indicating that the metamorphic recrystallization took place at much lower temperatures with subsequent slight amounts of exsolution during further cooling. There seems no question that the pigeonite and orthopyroxene lamellae exsolved at a temperature well below that of the pigeonite-orthopyroxene inversion curve. Two hypotheses are suggested as possible explanations: (1) Nucleation and growth within the monoclinic structure of the augite host favors metastable formation of pigeonite under conditions where orthopyroxene is the stable phase. (2) Pigeonite (or clinohypersthene) is again the stable phase at lower temperatures of exsolution (Kuno, 1966; Boyd and England, 1965; Sclar, Carrison, and Schwartz, 1964; Smith, 1969; Brown, 1968, 1972; Grover, 1972).

The hypothesis of metastable formation in the augite host is very attractive. The nucleation and growth of pigeonite lamellae, particularly "001" lamellae, requires only migration of the 6- and 8-coordinated cations without major disruption of the monoclinic tetrahedral network that would be required for formation of orthopyroxene. The hypothesis of metastability allows simultaneous precipitation, for which there is some textural evidence, of pigeonite lamellae on "001" and orthopyroxene on (100) where the monoclinic and orthorhombic lattices have their best mutual fits respectively.

Simultaneous precipitation of pigeonite on "100" is also a possibility. This explanation would also be applicable to metamorphic rocks containing coexisting calcic clinoamphibole and orthoamphibole, in which the exsolution lamellae in the calcic amphibole are always monoclinic cummingtonite (Ross, Papike, and Shaw, 1969).

A further argument favoring metastable formation has to do with the optimal phase boundary theory itself. Orthopyroxene can have a good fit on augite only on (100), and this only provided the c and b dimensions of the two phases are nearly identical. Pigeonite, because of its monoclinic lattice, can achieve nearly perfect dimensional fit with both "001" and "100" lamellae provided it has a b dimension in common with the host. Indeed, the potential for better fit of pigeonite on irrational "100" planes as compared to poor fit of orthopyroxene on (100) could be used to explain the relative abundance of pigeonite "100" lamellae in most specimens.

In the case of the most iron-rich specimens (Po-13, Sc-6, Po-17), the argument given in the preceding paragraph can be reversed. In these specimens the fine "100" pigeonite lamellae are essentially parallel to (100) and to coarser (100) orthopyroxene lamellae (Table 1, Fig. 7), so that there is little or no misfit of the c dimensions of pigeonite and augite host. In this case one might ask what advantage monoclinic pigeonite essentially on (100) would have over orthopyroxene on (100) and consider again the possibility that the pigeonite is indeed the stable phase under the lowest exsolution temperatures.

Summary and Conclusions

1. In augites of augite-orthopyroxene pairs believed to have exsolved in a metamorphic environment there is a strong correlation between the angles of pigeonite "001" and "100" exsolution lamellae and the iron-magnesium ratio, with the largest angles in the most magnesian augites.

2. The angles of exsolution lamellae with respect to the a and c crystallographic axes are related to the misfits of the a and c lattice parameters and differences between the β angles of host and lamellae. In magnesian specimens misfits of a and c are *larger,* differences between β angles are *smaller.*

3. The optically measured angles of the exsolution lamellae are in close agreement with the angles

of optimal phase boundaries calculated from lattice parameters of augite host and pigeonite lamellae. In the most magnesian specimens relative lattice rotations measured from precession photographs are in nearly exact agreement with relative lattice rotations calculated from lattice parameters. These two facts give strong evidence that the pigeonite lamellae nucleated on "optimal phase boundaries" and that the relative lattice parameters of host and lamellae have not changed a great deal since nucleation of lamellae under metamorphic conditions. This is in stark contrast to relations observed in some igneous pyroxenes (Ross *et al*, 1972).

4. A simple notation has been devised making use of irrational Miller indices that succinctly describes the orientation of the phase boundaries.

5. Pigeonite lamellae in augite hosts coexisting with orthopyroxene clearly exsolved below the pigeonite-orthopyroxene inversion temperature. It is not clear whether pigeonite nucleated metastably in augite hosts because of best fit considerations or whether pigeonite is again the stable phase under conditions of low temperature exsolution.

Appendix: Description of Specimens and Their Geologic Setting

Hudson Highlands

The Hudson Highlands of New York consist of a belt of high-grade, regionally metamorphosed, essentially concordant, Precambrian gneisses and granulites that represent a northeastern extension of the Reading Prong and the Blue Ridge geomorphic and petrographic provinces. According to Jaffe and Jaffe (1973), the gneisses and granulites of the Hudson Highlands represent a eugeosynclinal sequence of sedimentary and volcanic rocks that attained a largely isochemical metamorphic equilibrium under conditions of the hornblende granulite facies. According to these authors metamorphism took place at temperatures of 700–800°C and pressures in the range of 2–4 kbar under relatively dry conditions with P_{H_2O} considerably lower than P_{Total}. Similar estimates were obtained by Dodd (1965) and Dallmeyer and Dodd (1971) from a study of mineral assemblages in adjoining terrane. Exsolution in pyroxenes, as well as in feldspars, of necessity commenced below these maxima, although not necessarily much below these values. A further episode of unmixing in the solid state at still lower T and P conditions could have occurred in Paleozoic and/or Triassic time associated with orogenic events that mildly affected this region (Hall, 1968). Variation in exsolution textures, such as irregularities in size, distribution, and percentages of both "001", "100" pigeonite, and (100) hypersthene lamellae in grains of host augite, from the same small specimen suggest that solid state exsolution may have taken place in more than one stage.

J-241S. Pyroxene plagioclase granulite, similar to J-437P, below.

J-515. Orthopyroxene-quartz-andesine gneiss, quartz 33%, K-feldspar 1%, andesine (An$_{39}$) 55%, orthopyroxene 8%, augite 1%, biotite 1%, magnetite 1%.

J-223. Equigranular pyroxene granulite, orthopyroxene 30%, augite 50%, hornblende 5%, quartz 15%.

J-437P. Pyroxene plagioclase granulite, andesine (An$_{32}$) 65%, orthopyroxene 16%, augite 11%, hornblende 1%, magnetite 4%, quartz 1%, K-feldspar 2%.

Adirondacks

The Adirondack province of northern New York consists of a circular area of Precambrian crystalline rocks that occupy approximately 30,000 square kilometers (Fig. 1). The northeastern quarter of this circular region contains a heart-shaped massif of anorthosite, intimately associated with charnockitic gneiss and minor amounts of gneiss and granulite of sedimentary and volcanic ancestry (Kemp, 1921; Buddington, 1939; Crosby, 1969; de Waard, 1970, Davis, 1971). All of the exsolved pyroxenes from the Adirondack region described in this report are from this anorthosite-charnockite complex (Table 1, Fig. 2).

Metamorphic relations in the anorthosite-charnockite complex of the northeast Adirondacks are complicated by the coexistence of apparent pyroxene-hornfels facies contact metamorphic assemblages (Turner, 1968, p. 224, 235, 242) such as calcite-monticellite-forsterite-augite-garnet-spinel and wollastonite-diopside-grossular with granulite facies regional metamorphic assemblages such as orthopyroxene-augite-garnet-plagioclase and quartz-calcite-diopside-grossular. It is not yet known whether the former represent contact metamorphic assemblages formed by anorthosite magma in contact with argillaceous dolomite that has survived the later regional granulite facies metamorphism or whether these assemblages resulted from special localized conditions of low activity of CO_2 that may have existed during regional metamorphism (Walter, 1963). The extremely iron-rich orthopyroxenes reported here suggest, according to the experimental data of Smith (1971), that pressures may have been in excess of 7 kbar.

Jo-8. Anorthositic gabbro, sub-ophitic; andesine (An$_{46}$) 57%, andesine antiperthite 19%, augite 17%, orthopyroxene 5%, ilmenite + biotite + apatite 2%.

Ph-3, IV-A1, MD-1, VI-Nk. Similar to Jo-8.

Pr-1 and CD. Gabbroic anorthosite; andesine (An$_{46}$), garnet, orthopyroxene, augite, hornblende, ilmenite, magnetite in a matrix of andesine and minor K-feldspar.

Go-4. Pyroxenite; augite 65%, orthopyroxene 25%, andesine 3%, microperthite 3%, quartz 3%, magnetite 1/2%, biotite 1/2%.

Ma-5. Similar to Go-4.

Po-1. Gabbroic anorthosite gneiss; andesine (An$_{48}$) megacrysts 13% in a matrix of andesine (An$_{44}$) 58%, orthoclase 6%, augite 7%, orthopyroxene 3%, hornblende 4%, garnet 3%, ilmenite 4%, magnetite 1%, apatite 1%.

Sb-2, S1-5, VH-1, VH-2. Similar to Po-1.

Ca-6. Melagabbro granulite; andesine 28%, microperthite 5%, orthopyroxene 23%, augite 11%, garnet 10%, ilmenite 13%, magnetite 4%, apatite 6%.

Ma-3. Similar to Ca-6.

Ca-17. Microperthite-pyroxene granulite; microperthite 50%, orthopyroxene 15%, augite 35%.

Jb-2. Microperthite granulite; blue megacrysts of microperthite in a matrix of oligoclase (An$_{26}$), orthopyroxene, augite, garnet, magnetite, ilmenite, apatite.

Po-13. Ferromangerite gneiss; microperthite 37%, oligoclase (An$_{23}$) 33%, quartz 4%, augite 6%, orthopyroxene 4%, hornblende 4%, garnet 7%, magnetite + ilmenite 3%, apatite 2%.

Go-2, SC-6, Po-17, Giant, Sb-1. Similar to Po-13.

Belchertown Complex

The pyroxene-bearing specimens from the Belchertown Intrusive Complex are from the extreme inner portion of the batholith that has largely escaped major metamorphic hydration during the Acadian kyanite-grade regional metamorphism that affected the country rocks. The pyroxene-bearing rocks thus represent an igneous mineralogy that has undergone a slight but as yet uncertain degree of metamorphic recrystallization. The fact that pelitic schist inclusions in the hydrated part of the batholith up to hundreds of feet thick and several miles long contain sillimanite (and sillimanite pseudomorphs of andalusite) shows that the batholith strongly disturbed the local thermal structure and that metamorphic hydration and recrystallization took place at metamorphic temperatures considerably above those of the kyanite zone. The specimens are from two localities collected by David J. Hall (1973) in a regional study of geophysics and petrography, and the mineralogy and petrology of both are being studied in greater detail by Lewis D. Ashwal (1974). The extremely magnesian compositions of the pyroxenes from the Belchertown monzodiorites as compared to rocks of comparable feldspar composition in the Adirondacks appear to be due to the extremely high activity of oxygen under which they crystallized, as indicated by the presence of primary high temperature titano-hematite.

447. Core of ultramafic inclusion 700 feet across described by Emerson (1898, 1917) as "cortlandtite;" very coarse augite 50–75%, pargasite 10–40%, and orange-brown biotite 3–14% enclosing grains of augite, orthopyroxene 1–7%, olivine (Fa$_{11}$, γ = 1.694) 5% and rutile.

113, 115, 110, A21. Pyroxene monzodiorites typical of core of batholith; clouded pink oligoclase (An$_{26-29}$) 40–47%, orthoclase microperthite 11–18%, quartz 4–13%, augite 7–18%, orthopyroxene 4–8%, hornblende 0.5–2%, biotite 6–14%, titanohematite and magnetite 0.5–1.0%.

Cortlandt Complex

The Cortlandt Complex near Peekskill, New York, is a mafic to ultramafic layered intrusion of probable Ordovician age, according to Long and Kulp (1962). It is intruded into sillimanite-grade schists and gneisses of the northern Manhattan Prong and displays a thermal metamorphic aureole. Ratcliffe (1968) suggested that the Complex was intruded after most Taconic age deformation and metamorphism had occurred. Tracy (1970) found features

in the eastern, ultramafic end of the complex indicative of later metamorphic recrystallization such as alteration of pyroxenes to hornblende and biotite, and exsolution of pyroxenes and oxide phases. This was ascribed to an Acadian reheating event, proposed by Long and Kulp (1962) to account for hybrid K-Ar ages in the Manhattan Prong.

T62, T58, T52, T65. Olivine pyroxenites; orthopyroxene 20–40%, augite 30–50%, olivine (Fa_{20}) 5–35%.

T25. Hornblende-biotite pyroxenite; orthopyroxene 40%, augite 30%, hornblende 16%, biotite 8%, minor serpentine probably after olivine.

Acknowledgments

References

ASHWAL, L. D. (1974) *Metamorphic Hydration of Augite-Orthopyroxene Monzodiorite to Hornblende Granodiorite Gneiss, Belchertown Batholith, Massachusetts.* M.S. Thesis, University of Massachusetts, 116 p.

BOLLMANN, W. (1970) *Crystal Defects and Crystalline Interfaces.* Springer, Berlin.

———, AND H. -U. NISSEN (1968) A study of optimal phase boundaries: the case of exsolved alkali feldspars. *Acta Crystallogr.* A24, 546–557.

BOYD, F. R., AND G. M. BROWN (1968) Electron-probe study of exsolution in pyroxenes. *Carnegie Inst. Wash. Year Book,* 66, 353–359.

———, AND ——— (1969) Electron-probe study of pyroxene exsolution. *Mineral. Soc. Am. Spec. Pap.* 2, 211–216.

———, AND J. L. ENGLAND (1965) The rhombic enstatite-clinoenstatite inversion. *Carnegie Inst. Wash. Year Book,* 64, 116–120.

BROWN, G. M. (1968) Experimental studies on inversion relations in natural pigeonite pyroxenes. *Carnegie Inst. Wash. Year Book,* 66, 347–353.

——— (1972) Pigeonite pyroxenes: A review. *Geol. Soc. Am. Mem.* 132, 523–534.

BUDDINGTON, A. F. (1939) Adirondack igneous rocks and their metamorphism. *Geol. Soc. Am. Mem.* 7, 354 p.

CROSBY, PERCY (1969) Petrogenetic and statistical implications of modal studies in Adirondack anorthosite. *N.Y. State Mus. Sci. Serv. Mem.* 18, 289–304.

DALLMEYER, R. D., AND R. T. DODD (1971) Distribution and significance of cordierite in paragneisses of the Hudson Highlands, southeastern New York. *Contrib. Mineral. Petrol.* 33, 289–308.

DAVIS, B. T. C. (1971) Bedrock geology of the St. Regis quadrangle, New York. *N. Y. State Mus. Sci. Serv., Map and Chart Ser. No.* 16, 34 p.

DEER, W. A., R. A. HOWIE, AND JACK ZUSSMAN (1963) *Rock-Forming Minerals,* Vol. 2, *Chain Silicates.* John Wiley and Sons, New York, 379 p.

DE WAARD, DIRK (1970) The anorthosite-charnockite suite of rocks of Roaring Brook Valley in the eastern Adirondacks (Marcy Massif). *Am. Mineral.* 55, 2063–2075.

DODD, R. T., JR. (1965) Precambrian geology of the Popolopen Lake Quadrangle, southeastern New York. *New York State Mus. and Sci. Serv., Map and Chart Ser. No.* 6, 39 p.

EMERSON, B. K. (1898) Geology of Old Hampshire County, Massachusetts comprising of Franklin, Hampshire, and Hampden Counties. *U.S. Geol. Surv. Mon.* 29, 790 p.

——— (1917) Geology of Massachusetts and Rhode Island. *U.S. Geol. Surv. Bull.* 597, 289 p.

GROVER, JOHN (1972) The stability of low-clinoenstatite in the system $Mg_2Si_2O_6$–$CaMgSi_2O_6$. *Trans. Am. Geophys. Union,* 53, 539.

GUTHRIE, J. O. (1972) Geology of the northern portion of the Belchertown Intrusive Complex, west-central Massachusetts. *Geol. Dept., Univ. Mass., Contrib. No.* 8, 110 p.

———, AND PETER ROBINSON (1967) Geology of the northern portion of the Belchertown Intrusive Complex. *Guidebook for Field Trips in the Connecticut Valley of Massachusetts, 59th Annu. Meet., New England Intercollegiate Geol. Conf., Amherst, Mass.,* p. 143–153.

HALL, D. J. (1973) *Geology and Geophysics of the Belchertown Batholith, West-Central Massachusetts.* Ph.D. Thesis, University of Massachusetts, 110 p.

HALL, L. M. (1968) Times of origin and deformation of bedrock in the Manhattan Prong. In, E-an Zen, and W. S. White, Eds., *Studies of Appalachian Geology: Northern and Maritime.* John Wiley and Sons, New York. 117–127.

HESS, H. H. (1949) Chemical composition and optical properties of clinopyroxenes. *Am. Mineral.* 34, 621–666.

——— (1952) Orthopyroxenes of the Bushveld type, ion substitutions, and changes in unit cell dimensions. *Am. J. Sci., Bowen Vol.,* 173–187.

——— (1960) Stillwater igneous complex, Montana. *Geol. Soc. Am. Mem.* 80, 230 p.

HOWIE, R. A. (1955) The geochemistry of the charnockite series of Madras. *Trans. Roy. Soc. Edinburgh,* 62, 725–768.

JAFFE, H. W., AND E. B. JAFFE (1973) Bedrock geology of the Monroe quadrangle, New York. *N.Y. State Museum and Sci. Serv., Map and Chart Ser. No.* 20, Albany, N.Y.

——, PETER ROBINSON, AND CORNELIS KLEIN, JR. (1968) Exsolution lamellae and optic orientation of clinoamphiboles. *Science, 160,* 776–778.

KEMP, J. F. (1921) Geology of the Mount Marcy quadrangle, New York. *N.Y. State Mus. Bull.* **229–230,** 86 p.

KRETZ, RALPH (1963) Distribution of magnesium and iron between orthopyroxene and calcic pyroxene in natural mineral assemblages. *J. Geol.* **71,** 773–785.

KUNO, HISASHI (1954) Study of orthopyroxenes from volcanic rocks. *Am. Mineral.* **39,** 30–46.

——(1966) Review of pyroxene relations in terrestrial rocks in the light of recent experimental work. *Mineral. J. (Tokyo),* 5, 21–43.

LINDSLEY, D. H., H. E. KING, JR., AND A. C. TURNOCK (1974) Compositions of synthetic augite and hypersthene coexisting at 810°C: Application to pyroxenes from lunar highlands rocks. *Geophys. Res. Lett.* **1,** 134–136.

LINDSLEY, D. H., I. D. MACGREGOR, AND B. T. C. DAVIS (1964) Synthesis and stability of ferrosilite. *Carnegie Inst. Wash. Year Book,* **63,** 174–176.

LONG, L. E., AND J. L. KULP (1962) Isotopic age study of the metamorphic history of the Manhattan and Reading Prongs. *Geol. Soc. Am. Bull.* **73,** 969–996.

MUIR, I. D., AND C. E. TILLEY (1958) The compositions of coexisting pyroxenes in metamorphic assemblages. *Geol. Mag.* **95,** 403–408.

POLDERVAART, ARIE, AND H. H. HESS (1951) Pyroxenes in the crystallization of basaltic magma. *J. Geol.* **59,** 472–489.

PRESTON, JOHN (1966) An unusual hourglass structure in augite. *Am. Mineral.* **51,** 1227–1233.

RATCLIFFE, N. M. (1968) Contact relations of the Cortlandt Complex at Stony Point, New York, and their regional implications. *Geol. Soc. Am. Bull.* **79,** 777–786.

ROBINSON, PETER, H. W. JAFFE, MALCOLM ROSS, AND CORNELIS KLEIN, JR. (1971) Orientation of exsolution lamellae in clinopyroxenes and clinoamphiboles: consideration of optimal phase boundaries. *Am. Mineral.* **56,** 909–939.

——, ——, ——, —— (1971) Erratum. *Am. Mineral.* **56,** 1836.

ROSS, MALCOLM, J. J. PAPIKE, AND K. W. SHAW (1969) Exsolution textures in amphiboles as indicators of sub-

solidus thermal histories. *Mineral. Soc. Am. Spec. Pap.* **2,** 275–299.

——, PETER ROBINSON, AND H. W. JAFFE (1972) Pigeonite lamellae in Bushveld augite sequentially exsolved on phase boundaries at angles controlled by differential thermal contraction. *Geol. Soc. Amer. Abstracts with Programs 1972,* 644–645.

——, J. S. HUEBNER, AND ERIC DOWTY (1973) Delineation of the one atmosphere augite-pigeonite miscibility gap for pyroxenes from lunar basalt 12021. *Amer. Mineral.* **58,** 619–635.

SAXENA, S. K. (1971) Mg^{2+}-Fe^{2+} order-disorder in orthopyroxene and the Mg^{2+}-Fe^{2+} distribution between coexisting minerals. *Lithos,* **4,** 345–356.

SCLAR, C. B., L. C. CARRISON, AND C. M. SCHWARTZ (1964) High-pressure stability field of clinoenstatite and the orthoenstatite-clinoenstatite translation (abstr.). *Trans. Am. Geophys. Union.* **45,** 121.

SHAND, S. J. (1942) Phase petrology of the Cortlandt Complex, New York. *Geol. Soc. Am. Bull.* **53,** 409–428.

SMITH, DOUGLAS (1971) Stability of the assemblage iron-rich orthopyroxene-olivine-quartz. *Am. J. Sci.* **271,** 370–382.

SMITH, J. V. (1969) Crystal structure and stability of the $MgSiO_3$ polymorphs; physical properties and phase relations of Mg, Fe pyroxenes. *Mineral. Soc. Am. Spec. Pap.* **2,** 3–29.

STEPHENSON, D. A., C. B. SCLAR, AND J. V. SMITH (1966) Unit cell volumes of synthetic orthoenstatite and low clinoenstatite. *Mineral. Mag.* **35,** 838–846.

TRACY, R. J. (1970) *The Petrology of the Eastern End of the Cortlandt Complex, Westchester County, New York.* M.Sc. Thesis, Brown University, 45 p.

TURNER, F. J. (1968) *Metamorphic Petrology.* McGraw Hill, New York, 403 p.

TURNOCK, A. C., D. H. LINDSLEY, AND J. E. GROVER (1973) Synthesis and unit cell parameters of Ca-Mg-Fe pyroxenes. *Am. Mineral.* **58,** 50–59.

WALTER, L. S. (1963) Experimental studies on Bowen's decarbonation series. *Am. J. Sci.* **261,** 773–779.